Geochemistry Geophysics Geosystems G3

Article
Volume 11, Number 5
12 May 2010
Q05T09, doi:10.1029/2009GC002977
ISSN: 1525-2027

Published by AGU and the Geochemical Society

Geochemistry of lavas from the 2005–2006 eruption at the East Pacific Rise, 9°46′N–9°56′N: Implications for ridge crest plumbing and decadal changes in magma chamber compositions

A. R. Goss and M. R. Perfit
Department of Geological Sciences, University of Florida, 241 Williamson Hall, Gainesville, Florida 32611-2122, USA (argoss@ufl.edu; mperfit@ufl.edu)

W. I. Ridley
U.S. Geological Survey, Denver Federal Center, Box 25046, Denver, Colorado 80225, USA (iridley@usgs.gov)

K. H. Rubin
Department of Geology and Geophysics, SOEST, University of Hawai'i at Mānoa, 1680 East West Road, Honolulu, Hawaii 96822, USA (krubin@hawaii.edu)

G. D. Kamenov
Department of Geological Sciences, University of Florida, 241 Williamson Hall, Gainesville, Florida 32611-2122, USA (kamenov@ufl.edu)

S. A. Soule
Department of Geology and Geophysics, Woods Hole Oceanographic Institution, Mail Stop 24, Woods Hole, Massachusetts 02543, USA (ssoule@whoi.edu)

A. Fundis
Department of Geological Sciences, University of Florida, 241 Williamson Hall, Gainesville, Florida 32611-2122, USA (afundis@ufl.edu)

D. J. Fornari
Department of Geology and Geophysics, Woods Hole Oceanographic Institution, Mail Stop 24, Woods Hole, Massachusetts 02543, USA (dfornari@whoi.edu)

[1] Detailed mapping, sampling, and geochemical analyses of lava flows erupted from an ~18 km long section of the northern East Pacific Rise (EPR) from 9°46′N to 9°56′N during 2005–2006 provide unique data pertaining to the short-term thermochemical changes in a mid-ocean ridge magmatic system. The 2005–2006 lavas are typical normal mid-oceanic ridge basalt with strongly depleted incompatible trace element patterns with marked negative Sr and Eu/Eu* anomalies and are slightly more evolved than lavas erupted in 1991–1992 at the same location on the EPR. Spatial geochemical differences show that lavas from the northern and southern limits of the 2005–2006 eruption are more evolved than those erupted in the central portion of the fissure system. Similar spatial patterns observed in 1991–1992 lavas suggest geochemical gradients are preserved over decadal time scales. Products of northern axial and off-axis fissure eruptions are consistent with the eruption of cooler, more fractionated lavas that also record a parental melt compo-

nent not observed in the main suite of 2005–2006 lavas. Radiogenic isotopic ratios for 2005–2006 lavas fall within larger isotopic fields defined for young axial lavas from 9°N to 10°N EPR, including those from the 1991–1992 eruption. Geochemical data from the 2005–2006 eruption are consistent with an invariable mantle source over the spatial extent of the eruption and petrogenetic processes (e.g., fractional crystallization and magma mixing) operating within the crystal mush zone and axial magma chamber (AMC) before and during the 13 year repose period. Geochemical modeling suggests that the 2005–2006 lavas represent differentiated residual liquids from the 1991–1992 eruption that were modified by melts added from deeper within the crust and that the eruption was not initiated by the injection of hotter, more primitive basalt directly into the AMC. Rather, the eruption was driven by AMC pressurization from persistent or episodic addition of more evolved magma from the crystal mush zone into the overlying subridge AMC during the period between the two eruptions. Heat balance calculations of a hydrothermally cooled AMC support this model and show that continual addition of melt from the mush zone was required to maintain a sizable AMC over this time interval.

Components: 24,600 words, 11 figures, 6 tables.

Keywords: mid-ocean ridge basalt; East Pacific Rise; eruption; trace elements; radiogenic isotopes; fractional crystallization.

Index Terms: 1032 Geochemistry: Mid-oceanic ridge processes (3614, 8416); 1036 Geochemistry: Magma chamber processes (3618); 1021 Geochemistry: Composition of the oceanic crust.

Received 1 December 2009; **Revised** 8 March 2010; **Accepted** 12 March 2010; **Published** 12 May 2010.

Goss, A. R., M. R. Perfit, W. I. Ridley, K. H. Rubin, G. D. Kamenov, S. A. Soule, A. Fundis, and D. J. Fornari (2010), Geochemistry of lavas from the 2005–2006 eruption at the East Pacific Rise, 9°46′N–9°56′N: Implications for ridge crest plumbing and decadal changes in magma chamber compositions, *Geochem. Geophys. Geosyst.*, *11*, Q05T09, doi:10.1029/2009GC002977.

Theme: Recent Volcanic Eruptions, Properties, and Behavior of the Fast Spreading East Pacific Rise at 8°–11°N
Guest Editors: S. M. Carbotte, R. Haymon, and W. Seyfried

1. Introduction

[2] The 8°N–11°N segment of the EPR is one of the best characterized and most densely sampled regions of the global MOR system. Multidisciplinary mapping combined with reconnaissance geochemical studies have elucidated many of the tectonic, magmatic, and hydrothermal processes operating at this and other fast spreading centers [e.g., *Haymon et al.*, 1991; *Langmuir et al.*, 1992; *Macdonald et al.*, 1992; *Haymon et al.*, 1993; *Perfit et al.*, 1994a; *Von Damm et al.*, 1995; *Fornari et al.*, 1998; *Rubin et al.*, 2001; *Fornari et al.*, 2004]. Despite these and many other studies, our understanding of MOR volcanism at the fundamental scale of individual eruptions has been limited by the small number of studies that have determined the absolute ages of MOR lavas, distinguished between individual eruptive units, and/or evaluated their geochemical characteristics [*Rubin et al.*, 1994; *Gregg et al.*, 1996; *Perfit and Chadwick*, 1998; *Rubin et al.*, 2001; *Sinton et al.*, 2002; *Bergmanis et al.*, 2007]. Significant questions remain regarding the rates and scales of magmatic phenomena at fast spreading centers, specifically with respect to the interplay between eruption recurrence intervals, rates of magma crystallization/recharge in crustal reservoirs, and inputs of mantle-derived melt to the crust.

[3] Well-documented historical MOR volcanic eruptions are uncommon and have largely been confined to areas along the Juan de Fuca Ridge, Axial Seamount, the Galapagos Rift near 86.5°W, as well as a few areas on the northern and southern EPR, including the 9°50′N area of the northern EPR in 1991–1992 [*Haymon et al.*, 1993; *Rubin et al.*, 1994; *Gregg et al.*, 1996; *Perfit and Chadwick*, 1998; *Embley et al.*, 2000; *Shank et al.*, 2003]. The 2005–2006 eruption on the northern EPR marks the first observed repeat submarine eruption along any segment of the global MOR system. Clearly, more repeat eruptions have occurred but the lack of real-time volcanic monitoring at most MOR sites limits

our ability to assess volcanic periodicity along oceanic spreading centers.

[4] Prior to this event, *Perfit and Chadwick* [1998] estimated a recurrence interval along the EPR (~11 cm/yr full spreading rate [*Carbotte and Macdonald*, 1992]) of one eruption every ~10 years per kilometer of ridge axis based on the correlation of spreading rate with eruptive flow volume. The thirteen year repose interval between eruptions at this site is consistent with this predicted periodicity, and the colocation of the 1991–1992 and 2005–2006 eruptions permits a chemical comparison between lavas erupted from the same axial magma chamber (AMC) over this time interval.

[5] Though there are multiple volcanological similarities between the 2005–2006 and 1991–1992 eruptions, including fissure-controlled emplacement [*Fornari et al.*, 1998, 2004], aerial extent [*Gregg et al.*, 1996], temporal duration (~1 year [*Rubin et al.*, 1994]), and hydrothermal fluid and ecological perturbations [*Von Damm et al.*, 1995; *Shank et al.*, 1998], the 2005–2006 eruptions are believed to be four to five times more voluminous [*Soule et al.*, 2007]. Contacts between the 2005–2006 and older terrain mapped by *Soule et al.* [2007] suggest many of the 2005–2006 flow units were emplaced directly on top of, and now obscure, most of the 1991–1992 flow units. Preeruption seismic data [*Tolstoy et al.*, 2006], high-resolution mapping [*Soule et al.*, 2007] and high-precision ^{210}Po dating of lavas from the 2005–2006 EPR eruption [*Rubin et al.*, 2006, 2008] have resulted in this being the best spatially and temporally constrained submarine eruption yet to be investigated.

[6] Studies have shown that lavas from the EPR exhibit distinct chemical variability that yield first-order information with regard to magma storage conditions and lava emplacement mechanisms at fast spreading mid-ocean ridges [*Langmuir et al.*, 1986; *Reynolds et al.*, 1992; *Perfit et al.*, 1994a; *Perfit and Chadwick*, 1998; *Rubin et al.*, 2001; *Smith et al.*, 2001; *Sinton et al.*, 2002; *White et al.*, 2002; *Soule et al.*, 2005]. In this context, the 2005–2006 and 1991–1992 eruptions provide critical data needed to constrain poorly understood rates of chemical differentiation and recharge of MOR AMCs during and between eruptions. Furthermore, the 2005–2006 eruption provides conclusive evidence that off-axis eruptions do occur along the EPR [e.g., *Perfit et al.*, 1994b; *Alexander and Macdonald*, 1996; *Perfit and Chadwick*, 1998; *Sims et al.*, 2003], in this case contemporaneous with more voluminous on-axis eruptions [*Soule et al.*, 2007]. The 2005–2006 EPR eruption also presents a unique opportunity to evaluate both intraeruption and intereruption chemical variation at one site over a known time interval (~6–12 months), as well as the spatial and temporal variability of the subridge mantle source. Such studies are comparatively common at hot spots [e.g., *Garcia et al.*, 2000; *Vlastélic et al.*, 2005] and convergent margin volcanic centers [e.g., *Reagan et al.*, 1987], where recurrent volcanic events provide temporal and spatial information on magmatic evolution, but are virtually absent in MOR settings.

[7] We present new geochemical data (major and trace element analyses and Sr, Nd, and Pb isotopic ratios) on basaltic glasses formed during the 2005–2006 EPR eruption to assess the chemical heterogeneity of erupted lavas and to evaluate magmatic processes in the mantle and crust that may have occurred on a decadal time scale. Overall, these data provide a refined view of the magmatic processes occurring during the construction of oceanic crust at fast spreading centers. The geochemical data are interpreted within the context of the seismically imaged magma storage bodies beneath this segment of the EPR axis [e.g., *Detrick et al.*, 1987; *Harding et al.*, 1993; *Kent et al.*, 1993b; *Carbotte et al.*, 2008] and geophysical and geochemical models that likewise constrain the local structure of the AMC, the characteristics of the deeper crystal mush zone [*Sinton and Detrick*, 1992; *Natland and Dick*, 2001], and estimates of magma recharge rates [*Liu and Lowell*, 2009]. We show that melts produced during the 2005–2006 eruption were derived from the addition and mixing of more evolved melt from the lower crustal mush zone to the AMC, and not from simple fractional crystallization of the 1991 magma within the shallow subridge AMC or from the addition of hotter more primitive melt to the AMC. Furthermore, we document that the off-axis lava unit at 9°53.3′N–9°56.4′N [see *Soule et al.*, 2007] is compositionally distinct from other lavas from this eruption and discuss its genetic relationship relative to axial lavas erupted from the axial summit trough (AST) further south (~9°50′N).

2. The 2005–2006 EPR Eruption

2.1. Spatial and Morphologic Constraints

[8] The 2005–2006 eruption along the EPR between 9°46′N and 9°56′N (Figure 1) [*Tolstoy et al.*, 2006; *Cowen et al.*, 2007; *Soule et al.*, 2007] was centered at 9°50′N in a region previously designated as the "bull's eye" of the NSF Ridge2000 program (http://

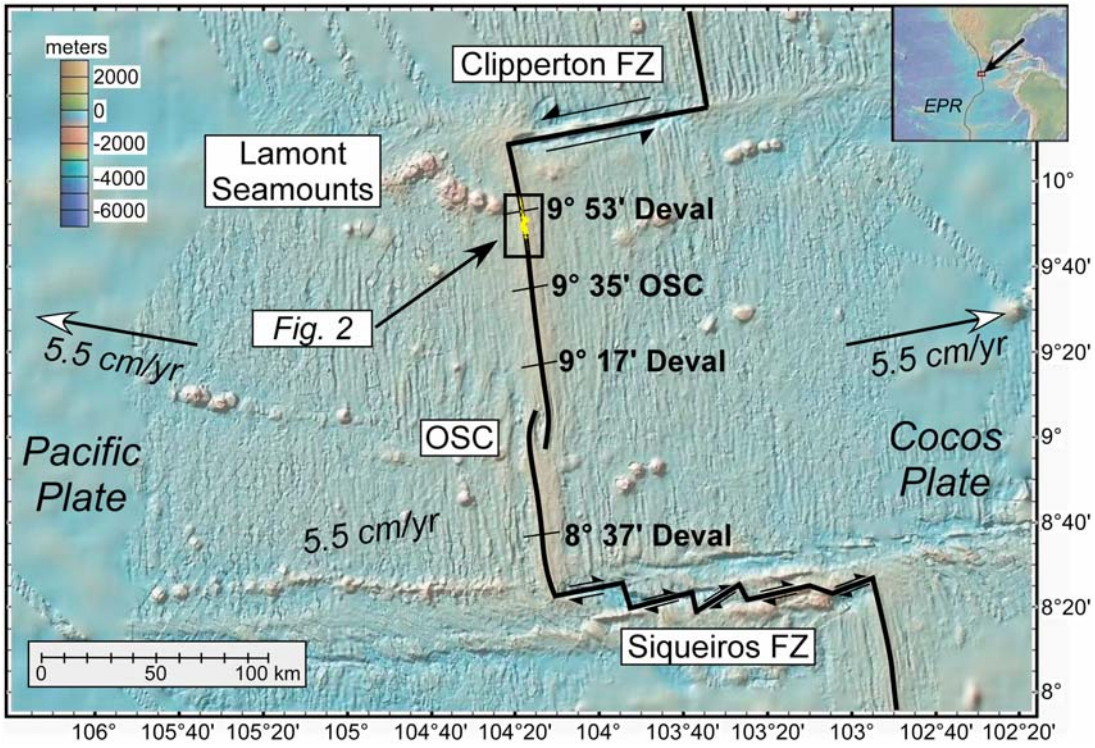

Figure 1. Bathymetric map of the 8°N–10°N region of the northern East Pacific Rise (EPR) showing the main ridge segments and transform faults. Bathymetric data are the 100 m resolution Global Multiresolution Topography (GMRT) data from the Marine Geoscience Data System (MGDS) database (http://www.marine-geo.org/ and references therein). Ridge segments are shown as solid black lines with the Clipperton and Siqueiros fracture zones marked by half arrows. Locations of deviations from axial linearity (devals) are also given [*Langmuir et al.*, 1986; *Kent et al.*, 1993b]. OSC, overlapping spreading center [see *Kent et al.*, 1993a]. Black box shows the location of the 2005–2006 eruption that is detailed in Figure 2. The dimensions of the young flow are shown in yellow within the box. Inset map gives location of the region along the northern EPR. Absolute spreading direction is shown by white arrows along with the half spreading rate [e.g., *Fornari et al.*, 1998].

www.ridge2000.org) EPR Integrated Study Site (ISS). Part of the motivation for choosing this site as an ISS was the extensive regional investigations following the spatially and temporally distinct 1991 ("tubeworm BBQ" at 9°50.6′N) and 1992 (9°53.3′N) EPR eruptions (see stars in Figure 2 for locations) [*Haymon et al.*, 1993; *Rubin et al.*, 1994; *Gregg et al.*, 1996; *Fornari et al.*, 2004] and the possibility that another eruption would occur during the Ridge2000 program. Initial indications of renewed magmatic activity and eruption of new lavas onto the seafloor included (1) discrete precursory chemical changes in hydrothermal vent fluids signifying enhanced magma-fluid interaction at depth [*Von Damm*, 2004]; (2) lost communication and poor recovery of ocean bottom seismometers (OBSs; 4 of 12 recovered) during an R/V *Knorr* cruise in April 2006 [*Tolstoy et al.*, 2006]; (3) excess particle turbidity and a complex bottom water thermal structure obtained by MAPR and CTD tows [*Cowen et al.*, 2007]; (4) very fresh lava obtained via along-axis dredging by the R/V *Knorr* at 9°48′N (A. Saal and D. Forsyth, personal communication, 2006), followed by TowCam seafloor imaging and additional dredging on

Figure 2. Bathymetric map of the 9°46′N–9°56′N segment of the northern East Pacific Rise showing the location of the axial summit trough (AST, gray area) and the spatial extent of the 2005–2006 eruption as determined from *Alvin* observations and TowCam photographic images [*Soule et al.*, 2007]. Sample locations (Table 1) are labeled, and colors show ranges of wt % MgO (Table 2). Stars show general loci of the 1991 BBQ (~9°50.6′N) and 1992 (~9°53.3′N) northern fissure eruptions. Black lines and blue fields delineate major off-axis faults and sheet flow filled lava channels, respectively. Flow fronts north of 9°52′N were dammed by a 10 m offset normal fault. Bathymetry is high-resolution EM 300 multibeam data from *White et al.* [2006]. Inset shows sample locations and compositions for 2005–2006 samples collected at/near the central region of the eruption. Samples D48-A and D48-B were collected by dredge by the R/V *Knorr*, with plotted locations representing the maximum length of the dredge track.

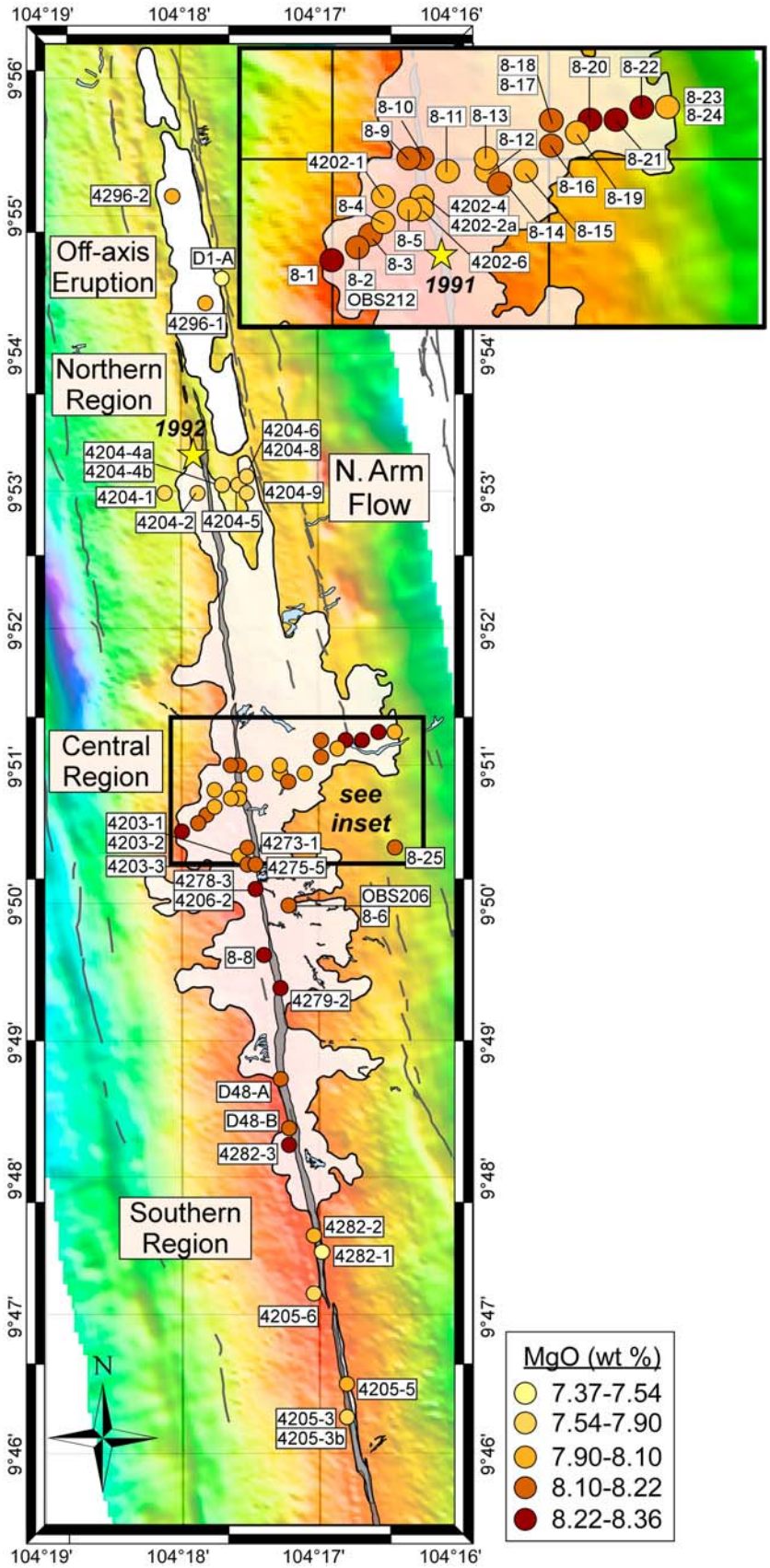
104°19'
104°18'
104°17'
104°16'
9°56'
9°55'
9°54'
9°53'
9°52'
9°51'
9°50'
9°49'
9°48'
9°47'
9°46'
Off-axis Eruption
Northern Region
Central Region
Southern Region
N. Arm Flow
1991
1992
see inset
4296-2
D1-A
4296-1
4204-4a
4204-4b
4204-1
4204-2
4204-5
4204-6
4204-8
4204-9
4203-1
4203-2
4203-3
4278-3
4206-2
4273-1
4275-5
8-25
OBS206
8-6
8-8
4279-2
D48-A
D48-B
4282-3
4282-2
4282-1
4205-6
4205-5
4205-3
4205-3b
8-18
8-17
8-20
8-22
8-23
8-24
8-10
8-11
8-13
8-9
8-12
8-21
4202-1
8-16
8-19
8-4
4202-4
4202-2a
8-14
8-15
8-5
8-3
4202-6
8-1
8-2
OBS212
N
MgO (wt %)
7.37-7.54
7.54-7.90
7.90-8.10
8.10-8.22
8.22-8.36

Figure 2

Table 1. Locations of Basalts From the 2005–2006 Eruption and Older Basalts From 9°39′N to 9°56′N[a]

Sample	Longitude (West)	Latitude (North)	Depth (m)	Age
		2005–2006 Eruption		
Central region (~9°49′N–9°51′N)				
Jason (J268) transect				
J268-1	104°17.977′	9°50.491′	2519	2005–2006
J268-2	104°17.893′	9°50.586′	2512	2005–2006
OBS 212	104°17.885′	9°50.575′	2462	2005–2006
J268-3	104°17.814′	9°50.642′	2511	2005–2006
J268-4	104°17.731′	9°50.722′	2506	2005–2006
J268-5	104°17.635′	9°50.775′	2504	2005–2006
J268-6	104°17.239′	9°49.985′	2505	2005–2006
OBS 206	104°17.231′	9°49.991′	2511	2005–2006
J268-8	104°17.427′	9°49.630′	2500	2005–2006
J268-9	104°17.623′	9°50.975′	2503	2005–2006
J268-10	104°17.585′	9°49.991′	2504	2005–2006
J268-11	104°17.456′	9°50.970′	2511	2005–2006
J268-12	104°17.308′	9°50.940′	2515	2005–2006
J268-13	104°17.283′	9°51.011′	2519	2005–2006
J268-14	104°17.207′	9°50.872′	2522	2005–2006
J268-15	104°17.088′	9°50.961′	2527	2005–2006
J268-16	104°16.983′	9°51.041′	2532	2005–2006
J268-17	104°16.967′	9°51.181′	2536	2005–2006
J268-18	104°16.989′	9°51.176′	2533	2005–2006
J268-19	104°16.888′	9°51.137′	2538	2005–2006
J268-20	104°16.808′	9°51.183′	2539	2005–2006
J268-21	104°16.681′	9°51.202′	2539	2005–2006
J268-22	104°16.532′	9°51.214′	2554	2005–2006
J268-23	104°16.417′	9°51.223′	2558	2005–2006
J268-24	104°16.442′	9°51.220′	2558	2005–2006
J268-25	104°16.442′	9°50.399′	2514	-
Alvin dives				
4202-1	104°17.743′	9°50.803′	2504	2005–2006
4202-2a	104°17.590′	9°50.793′	2503	2005–2006
4202-4	104°17.588′	9°50.793′	2504	2005–2006
4202-6	104°17.582′	9°50.737′	2504	2005–2006
4203-1	104°17.568′	9°50.328′	2500	2005–2006
4203-2	104°17.568′	9°50.328′	2500	2005–2006
4203-3	104°17.502′	9°50.273′	2505	2005–2006
4206-2	104°17.480′	9°50.105′	2502	2005–2006
4273-1	104°17.502′	9°50.405′	*2500*	2005–2006
4275-5	104°17.483′	9°50.306′	2506	2005–2006
4278-3	104°17.446′	9°50.113′	2503	2005–2006
4279-2	104°17.307′	9°49.396′	2498	2005–2006
Northern region (9°52′N–9°56′N)				
Axial				
4204-1	104°18.135′	9°52.954′	2559	2005–2006
4204-2	104°17.855′	9°52.998′	2559	2005–2006
4204-4a	104°17.689′	9°53.028′	2547	2005–2006
4204-4b	104°17.689′	9°53.028′	2547	2005–2006
Northern Arm Flow (NARF)				
4204-5	104°17.586′	9°53.060′	2546	2005–2006
4204-6	104°17.502′	9°53.095′	2545	2005–2006
4204-8	104°17.529′	9°53.078′	2545	2005–2006
4204-9	104°17.525′	9°52.965′	2545	2005–2006
Off axis				
D1-a	104°17.681′	9°54.522′	2556	2005–2006
4296-1	104°17.823′	9°54.346′	-	2005–2006
4296-2	104°18.035′	9°55.166′	-	2005–2006
Southern region (9°46′N–9°49′N)				
Axial				
4205-3	104°16.793′	9°46.257′	2526	2005–2006
4205-3b	104°16.793′	9°46.257′	2526	2005–2006
4205-5	104°16.828′	9°46.525′	2523	2005–2006

Table 1. (continued)

Sample	Longitude (West)	Latitude (North)	Depth (m)	Age
4205-6	104°17.011′	9°47.169′	2510	2005–2006
4282-1	104°16.897′	9°47.438′	2507	2005–2006
4282-2	104°17.034′	9°47.587′	2506	2005–2006
4282-3	104°17.209′	9°48.262′	2501	2005–2006
D48-A	104°17.274′	9°48.730′	-	2005–2006
D48-B	104°17.218′	9°48.360′	-	2005–2006
		Older Lavas (Pre-2005)		
Central region (BBQ flow)				
2392-9	104°17.520′	9°50.580′	2524	1991
2372-1	104°17.522′	9°50.601′	2521	1991
2372-1[b]	104°17.522′	9°50.601′	2521	1991
2504-1	104°17.481′	9°50.303′	2515	1991
2368-4	104°17.625′	9°50.136′	2522	1991
2351-2RE	104°17.454′	9°50.924′	2514	1991
Northern region				
4204-3	104°17.688′	9°53.030′	2547	-
2359-4	104°17.868′	9°53.274′	2558	<1991
2497-1b	104°17.848′	9°53.264′	2555	1992
2497-5	104°17.952′	9°53.994′	2572	1992
Southern region				
4205-1	104°16.787′	9°46.249′	2519	-
4205-7	104°17.045′	9°47.244′	2512	-
4280-1	104°15.721′	9°39.281′	2534	-
4280-3	104°15.713′	9°39.535′	2544	-
4280-4	104°15.764′	9°39.750′	2543	-

[a]Twenty-seven rock samples were collected in June 2006 during the RESET06 cruise (R/V *Atlantis*, AT15-06), 10 were collected during a cruise in November–December 2006 (R/V *Atlantis*, AT15-13), 2 northernmost samples were collected during the LADDER-2 cruise in December 2006 (RV *Atlantis*, AT15-14), and 26 samples were collected with the ROV *Jason2* (Dive 268) during a cruise in April 2007 (R/V *Atlantis*, AT15-17). These are in addition to three dredge samples recovered during two other cruises in April (R/V *Knorr*, KN182-13) and May 2006 (R/V *New Horizon*, TCS06NH). Italicized depths are estimated from adjacent samples. Dash indicates no information is known.
[b]Replicate analysis.

the R/V *New Horizon* [*Cowen et al.*, 2007]; and (5) increasing levels of microseismicity [*Tolstoy et al.*, 2006; *Stroup et al.*, 2007].

[9] *Soule et al.* [2007] documented the spatial extent of the 2005–2006 EPR eruption (Figures 1 and 2) based on TowCam [*Fornari*, 2003] imaging surveys (R/V *New Horizon*, NH06 and R/V *Atlantis*, AT15-6, AT15-13, and AT15-27) and initial observations made using *Alvin* during the RESET06 response cruise (June–July 2006). They reported that the new flows cover 14.6 km^2 of seabed, with eruption products extending ~18 km along the EPR crest from at least 9°46′N to 9°56′N. The southern terminus of the flow is at 9°46′N, but the effects of the magmatic event were likely felt as far south as 9°39.5′N, where a new hydrothermal vent that produced vapor phase fluids was subsequently identified in November 2006 (K. von Damm, personal communication, 2007). Lava flow thicknesses away from flat-lying lava channels range from 1 to 2 m, with an average of 1.5 m, from which *Soule et al.* [2007] calculated an erupted volume of 22×10^6 m^3. This volume places the 2005–2006 EPR eruption within the upper third of known eruption volumes on intermediate to fast spreading ridges [e.g., *Sinton et al.*, 2002; *Rubin and Sinton*, 2007]. Based on previous geophysical estimates of AMC dimensions [e.g., *Harding et al.*, 1993; *Kent et al.*, 1993b], *Soule et al.* [2007] estimated the total volume of erupted magma was <15% of the available AMC melt volume (assuming no new magma was added), leading to the conclusion that the AMC was not substantially depleted at the end of the eruption.

[10] Four distinct regions of the lava flow are used here to spatially characterize the emplacement conditions of the 2005–2006 EPR eruption (Figure 2). First, the central region (9°49′N–9°51′N) contains the thickest and most voluminous flows, which erupted from a continuous axial fissure. Second, smaller axial eruptions north of 9°53′N were erupted from a discontinuous group of fissures into a deeply faulted terrain that generally inhibited flow away from the ridge axis. However, included in this northern group is a flow sourced from the axis, herein referred to as the Northern Arm Flow (NARF, Figure 2), that flowed ~750 m to the east where it was directed northward by a ~10–15 m high inward

facing ridge-parallel normal fault. The NARF is one aspect of the lava flow map presented here that differs from that of *Soule et al.* [2007], where this feature was interpreted as sourced from off-axis vents. The newer interpretation is based primarily on observations of flow channels from high-resolution side-scan imagery (S. A. Soule et al., manuscript in preparation, 2010). Third, off-axis lavas were erupted from fissures located ~600 m east of the ridge axis near 9°54.5′N. Flows from these fissures were constrained on the west by older volcanic constructional features originally sourced at the ridge crest and to the east by the aforementioned normal fault scarp [*Soule et al.*, 2007]. Observations and bathymetric profiles indicate the off-axis fissures sit atop a ~10 m high mound, but the newest flows themselves likely only comprise the top 1 to 1.5 m [*Soule et al.*, 2007]. The fourth area comprises the southern limit of the eruption south of 9°49′N and extends to 9°46′N, where discontinuous lavas erupted from axial fissures in the AST with limited flow outside of the trough.

2.2. Temporal Constraints on the 2005–2006 Eruption

[11] The 2005–2006 EPR eruption was initially interpreted as a brief (few days to weeks long) eruptive event in late January 2006 based on a peak in local seismic activity followed by an abrupt waning of microseismicity [*Tolstoy et al.*, 2006] and corresponding thermal anomalies in hydrothermal vent fluids in the area (K. Von Damm, unpublished data, 2007). A subsequent study of acoustic T wave phases recorded by a regional autonomous hydrophone array has likewise been interpreted to have been produced during a short, intense eruption [*Dziak et al.*, 2009]. However, high-resolution eruption ages (±1–3 months) based on ^{210}Po-^{210}Pb disequilibria in 16 lava samples mostly collected during the June 2006 eruption response cruise (AT15-6) indicate that the eruption occurred between June 2005 and January 2006 [*Rubin et al.*, 2006] though a comparative analysis of the timing and geometry of lava eruption ages with details of the aforementioned records indicates that the eruption occurred in pulses, with most activity occurring from June to August 2005 [*Rubin et al.*, 2008].

3. Geochemical Results

[12] To evaluate the spatial and temporal geochemical variability of the 2005–2006 EPR eruption at 9°50′N a total of 65 lava samples were collected in situ using the submersible *Alvin*. Sample locations and descriptions are given in Table 1. All samples were extremely fresh basaltic lavas, without Fe-Mn coatings, and contained <2% vol. phenocrysts. In this context, they were visibly discernable from significantly older lavas [see *Soule et al.*, 2007] and great care was taken during sampling to distinguish older lavas from the 2005–2006 flow. Chips of aphyric basaltic glasses were analyzed for major elements and most were analyzed for trace elements (Table 2). A subset of 18 representative samples were chosen for radiogenic isotopic analysis based on geographic extent of the eruption, available high-resolution ^{210}Po age dating [*Rubin et al.*, 2006, 2008], and variation in their major and trace element compositions (Table 3). Detailed descriptions of all analytical methods are given in Appendix A.

3.1. Major Elements

[13] Lavas emplaced during the 2005–2006 eruption are typical normal mid-ocean ridge basalt (N-MORB) and moderately evolved (MgO = 7.3–8.4 wt %) compared to the large suite of analyzed lavas collected from 9°N to 10°N along the EPR (see Figure 3 and Table 2) [*Langmuir et al.*, 1986; *Batiza and Niu*, 1992; *Perfit et al.*, 1994a; M. R. Perfit et al., manuscript in preparation, 2010]. The 2005–2006 lavas, however, exhibit analytically significant chemical variability with respect to the major elements despite the presumed short (~6 months) duration and limited spatial extent over which the eruptions occurred. As shown in Figure 3, axial basalts from the central region, including a suite of samples along a lava flow channel across the ridge crest (*Jason* Dive 268; see Figure 2), are generally the least evolved of all units from the 2005–2006 eruption (MgO = 7.9–8.4 wt %, FeO = 9.4 –10.4 wt %, Al_2O_3 = 14.9–15.3 wt %, CaO = 11.6–12.2 wt %). Lavas sampled from the southern segment of the 2005–2006 flow field are elatively heterogeneous, overlapping with and extending to more evolved compositions (Figure 3) (MgO = 7.5–8.3 wt %, FeO = 9.5–10.2 wt %, Al_2O_3 = 14.9–15.3 wt %, CaO = 11.6–12.0 wt %) along expected crystal fractionation paths from the more primitive central region lavas. This is particularly evident in TiO_2 concentrations that reach 1.7 wt % in axial basalts from the southern region (Figure 3).

[14] Figure 3 also shows that axial and off-axis basalts sampled from the northern region are more evolved (MgO = 7.3–8.0 wt %, FeO = 9.8–10.3 wt %, TiO_2 = 1.5–1.6 wt %) than the central

Table 2 (Sample). Major and Trace Element Analyses for Basalts From the 2005–2006 EPR Eruption and Older Basalts From 9° 39′N to 9°56′N [The full Table 2 is available in the HTML version of this article]

	Sample											
	Central Region *Jason* Transect											
	J268-1	J268-2	OBS 212	J268-3	J268-4	J268-5	J268-6	OBS 206	J268-8	J268-9	J268-10	J268-11
SiO_2	50.09	50.11	49.96	50.11	50.21	50.10	49.97	49.97	49.95	49.95	49.94	50.14
Al_2O_3	15.01	14.99	15.28	14.96	14.89	14.88	15.18	15.17	15.17	15.07	15.16	15.06
FeO	9.77	9.74	9.74	9.79	10.01	9.96	9.66	9.81	9.67	9.83	9.79	9.90
MnO	0.19	0.19	0.16	0.20	0.20	0.19	0.17	0.19	0.18	0.19	0.19	0.19
MgO	8.25	8.24	8.20	8.16	8.02	8.04	8.19	8.21	8.26	8.16	8.17	8.06
CaO	12.12	12.09	12.14	12.00	11.81	11.82	12.16	12.08	12.11	11.94	12.06	11.89
Na_2O	2.60	2.60	2.55	2.64	2.74	2.72	2.59	2.59	2.59	2.64	2.57	2.64
K_2O	0.09	0.09	0.08	0.10	0.09	0.09	0.09	0.09	0.09	0.09	0.10	0.10
P_2O_5	0.10	0.13	0.12	0.12	0.13	0.13	0.13	0.12	0.12	0.13	0.12	0.12
Cl^-	-	-	-	-	-	-	-	-	-	-	-	-
Total	99.62	99.57	99.63	99.47	99.55	99.37	99.50	99.62	99.54	99.44	99.47	99.55
Mg #	60.1	60.1	60.0	59.7	58.8	59.0	60.2	59.9	60.4	59.7	59.8	59.2
CaO/Al_2O_3	0.81	0.81	0.79	0.80	0.79	0.79	0.80	0.80	0.80	0.79	0.80	0.79
$(K_2O/TiO_2)*100$	6.69	6.68	6.08	6.92	6.48	6.46	6.57	6.57	6.29	6.28	7.16	6.86
Sc	39.4	42.5	41.6	41.6	42.3	42.0	41.7	42.6	41.9	43.9	42.3	42.3
Ti	12783	13504	13180	13490	14196	13980	13161	13261	13196	14167	13705	13882
V	271	288	280	286	297	293	283	282	281	300	292	294
Cr	275	292	286	283	242	247	297	298	298	267	272	259
Co	38.6	41.2	40.5	40.9	40.9	40.7	40.5	41.0	40.7	42.2	40.8	40.9
Ni	95.2	100.0	99.5	98.6	95.4	95.2	99.4	100.7	99.4	99.6	99.2	97.4
Cu	68.4	71.5	71.3	71.6	69.2	69.6	72.8	72.8	72.1	72.4	72.2	70.9
Zn	75.2	79.7	76.7	77.9	80.2	79.2	78.5	77.2	76.0	81.1	82.1	81.0
Ga	15.4	16.4	16.3	16.5	16.8	16.5	16.2	16.6	16.5	17.2	16.3	16.5
Rb	0.91	0.99	0.97	0.93	0.97	0.96	0.95	0.98	0.95	1.00	0.99	0.98
Sr	108	115	113	116	116	114	116	116	118	119	118	115
Y	30.0	32.0	31.1	31.7	33.6	32.9	31.1	31.2	31.0	33.7	32.4	32.8
Zr	83.3	87.4	86.0	87.7	91.9	90.3	85.0	85.5	85.1	92.2	88.2	90.1
Nb	2.11	2.22	2.19	2.18	2.24	2.21	2.14	2.17	2.15	2.28	2.20	2.22
Ba	8.43	8.96	8.69	8.64	8.57	8.76	8.66	8.64	8.42	8.80	8.84	8.56
La	3.11	3.33	3.27	3.31	3.39	3.35	3.31	3.27	3.25	3.44	3.34	3.36
Ce	9.88	10.46	10.14	10.45	10.78	10.65	10.32	10.21	10.19	10.87	10.57	10.60
Pr	1.67	1.77	1.75	1.76	1.84	1.82	1.75	1.76	1.75	1.85	1.80	1.82
Nd	9.05	9.72	9.40	9.70	10.10	9.95	9.55	9.47	9.43	10.08	9.85	9.81
Sm	3.09	3.27	3.19	3.26	3.40	3.36	3.22	3.22	3.19	3.46	3.33	3.39
Eu	1.13	1.20	1.16	1.19	1.24	1.23	1.19	1.18	1.17	1.25	1.21	1.23
Gd	4.44	4.38	4.53	4.29	4.36	4.46	4.47	4.52	4.50	4.42	4.47	4.44
Tb	0.76	0.80	0.77	0.79	0.84	0.82	0.79	0.78	0.78	0.84	0.82	0.83
Dy	4.88	5.14	4.99	5.15	5.42	5.33	5.08	5.01	5.01	5.40	5.24	5.31
Ho	1.04	1.11	1.07	1.10	1.16	1.14	1.10	1.08	1.07	1.16	1.12	1.13
Er	2.99	3.17	3.10	3.19	3.38	3.30	3.13	3.13	3.14	3.36	3.24	3.28
Tm	0.46	0.48	0.47	0.48	0.51	0.50	0.48	0.47	0.47	0.50	0.48	0.49
Yb	3.02	3.21	3.11	3.16	3.36	3.30	3.14	3.13	3.12	3.40	3.25	3.31
Lu	0.44	0.47	0.45	0.47	0.50	0.48	0.46	0.45	0.45	0.49	0.47	0.48
Hf	2.29	2.41	2.33	2.41	2.54	2.50	2.36	2.35	2.31	2.50	2.46	2.49
Ta	0.146	0.154	0.152	0.151	0.154	0.154	0.148	0.151	0.149	0.153	0.145	0.152
Pb	0.128	0.139	0.172	0.181	0.197	0.185	0.141	0.182	0.196	0.217	0.126	0.135
Th	0.121	0.130	0.129	0.131	0.133	0.129	0.132	0.128	0.130	0.133	0.133	0.134
U	0.053	0.056	0.056	0.055	0.057	0.056	0.056	0.056	0.055	0.058	0.057	0.056
Eu/Eu*	0.94	0.97	0.93	0.98	0.99	0.97	0.96	0.95	0.95	0.98	0.96	0.97
Zr/Y	2.78	2.73	2.76	2.76	2.74	2.75	2.74	2.74	2.74	2.73	2.72	2.75
Ce_N/Sm_N	0.80	0.80	0.79	0.80	0.79	0.79	0.80	0.79	0.80	0.79	0.79	0.78
Sm_N/Yb_N	1.14	1.13	1.14	1.15	1.13	1.13	1.14	1.14	1.14	1.13	1.14	1.14

Table 3. Sr, Nd, and Pb Isotopic Analyses From the 2005–2006 EPR (9°46′N–9°56′N) Eruption[a]

Sample	$^{87}Sr/^{86}Sr$	2σ	$^{143}Nd/^{144}Nd$	2σ	εNd	$^{208}Pb/^{204}Pb$	$^{207}Pb/^{204}Pb$	$^{206}Pb/^{204}Pb$	$^{208}Pb/^{206}Pb$
Central Region (9°49′N–9°51′N)									
4202-2a	0.702465	0.000010	0.5131790	0.0000038	10.6	37.663	15.472	18.249	2.064
4202-6	0.702501	0.000010	0.5131740	0.0000036	10.5	37.665	15.471	18.254	2.063
4203-2	0.702471	0.000010	0.5131750	0.0000048	10.5	37.679	15.473	18.263	2.063
4206-2	0.702470	0.000009	0.5131770	0.0000047	10.5	37.690	15.476	18.271	2.063
J268-15	-	-	-	-	-	37.673	15.472	18.258	2.063
J268-21	-	-	-	-	-	37.682	15.473	18.267	2.063
J268-21[b]	-	-	-	-	-	37.678	15.471	18.265	2.063
J268-24	-	-	-	-	-	37.681	15.472	18.266	2.063
North (9°52′N–9°53′N)									
4204-1	0.702490	0.000011	0.5131680	0.0000045	10.3	37.688	15.473	18.269	2.063
4204-2	0.702506	0.000010	0.5131800	0.0000046	10.6	37.692	15.474	18.269	2.063
4204-4a	0.702495	0.000007	0.5131670	0.0000052	10.3	37.691	15.474	18.270	2.063
4204-4b	0.702493	0.000010	0.5131650	0.0000072	10.3	37.686	15.472	18.269	2.063
4204-8	0.702522	0.000007	0.5131710	0.0000044	10.4	37.691	15.474	18.270	2.063
4204-9	0.702489	0.000012	0.5131930	0.0000053	10.8	37.691	15.473	18.269	2.063
North Off Axis									
4296-2	-	-	-	-	-	37.693	15.475	18.271	2.063
North: Older									
4204-3	0.702518	0.000010	0.5131620	0.0000044	10.2	37.733	15.478	18.314	2.060
4203-3 hi-L	-	-	-	-	-	37.736	15.479	18.316	2.060
South (9°46′N–9°47′N)									
4205-6	0.702505	0.000011	0.5131590	0.0000038	10.2	37.678	15.472	18.263	2.063
D48-A	0.702483	0.000010	0.5131670	0.0000043	10.3	37.687	15.474	18.270	2.063
D48-B	0.702486	0.000007	0.5131790	0.0000045	10.6	37.685	15.472	18.269	2.063

[a] 2σ reflects in-run machine error. Long-term reproducibility estimates are: $^{87}Sr/^{86}Sr$ = ±0.00003, $^{143}Nd/^{144}Nd$ = ±0.000018, $^{206}Pb/^{204}Pb$ = ±0.0034 (205 ppm), $^{207}Pb/^{204}Pb$ = 0.0028 (184 ppm), $^{208}Pb/^{204}Pb$ = ±0.0086 (234 ppm). See section A3 for details.
[b] Replicate analysis.

region lavas. These flows are geochemically similar to, though more homogeneous than, the southern flows. With the exception of a chemically anomalous dredged basalt D1-A, ^{210}Po-dated as having erupted during the 2005–2006 event (K. H. Rubin et al., unpublished data, 2008), northern region basalts have higher CaO (11.9–12.0 wt %) and lower Al_2O_3 (14.6–15.8 wt %) concentrations, and thus higher CaO/Al_2O_3 ratios compared to southern region basalts (Table 2). Basalts sampled from the northern arm flow (NARF; see Figure 3) also exhibit major element concentrations resembling axial basalts from the north rather than those erupted in the central region.

[15] In comparison to lavas from the 2005–2006 eruption, basalts from the 1991 BBQ eruption [*Perfit et al.*, 1994a; *Rubin et al.*, 1994; *Perfit and Chadwick*, 1998] are less evolved and include some of the most primitive samples collected within this fourth-order ridge segment (MgO = 8.4–8.7 wt %, FeO = 9.3–9.4 wt %, Al_2O_3 = 15.4–15.7 wt %, CaO = 12.0–12.9 wt %). These basalts also have lower TiO_2 concentrations and CaO/Al_2O_3 ratios than 2005–2006 lavas (Figure 3), consistent with their more primitive nature. It is important to note that lavas erupted in 1992 in the northern region near 9°53′N are more differentiated than 1991 BBQ lavas from the central region [*Rubin et al.*, 1994, 2001]. This is a similar spatial pattern to that observed in the 2005–2006 eruption, in that northern lavas are more evolved than those from the central region (Figure 3).

3.2. Trace Elements

[16] Normalized trace element concentrations in 2005–2006 basalts (Table 2 and Figure 4) show that all lavas exhibit smooth geochemical patterns characteristic of N-MORB with large ion lithophile element (LILE) and light REE depletions and flat middle to heavy REE patterns. Trace element enriched MORB signatures ($Ce_N/Yb_N \geq 1$) are absent in lavas from the 2005–2006 eruption

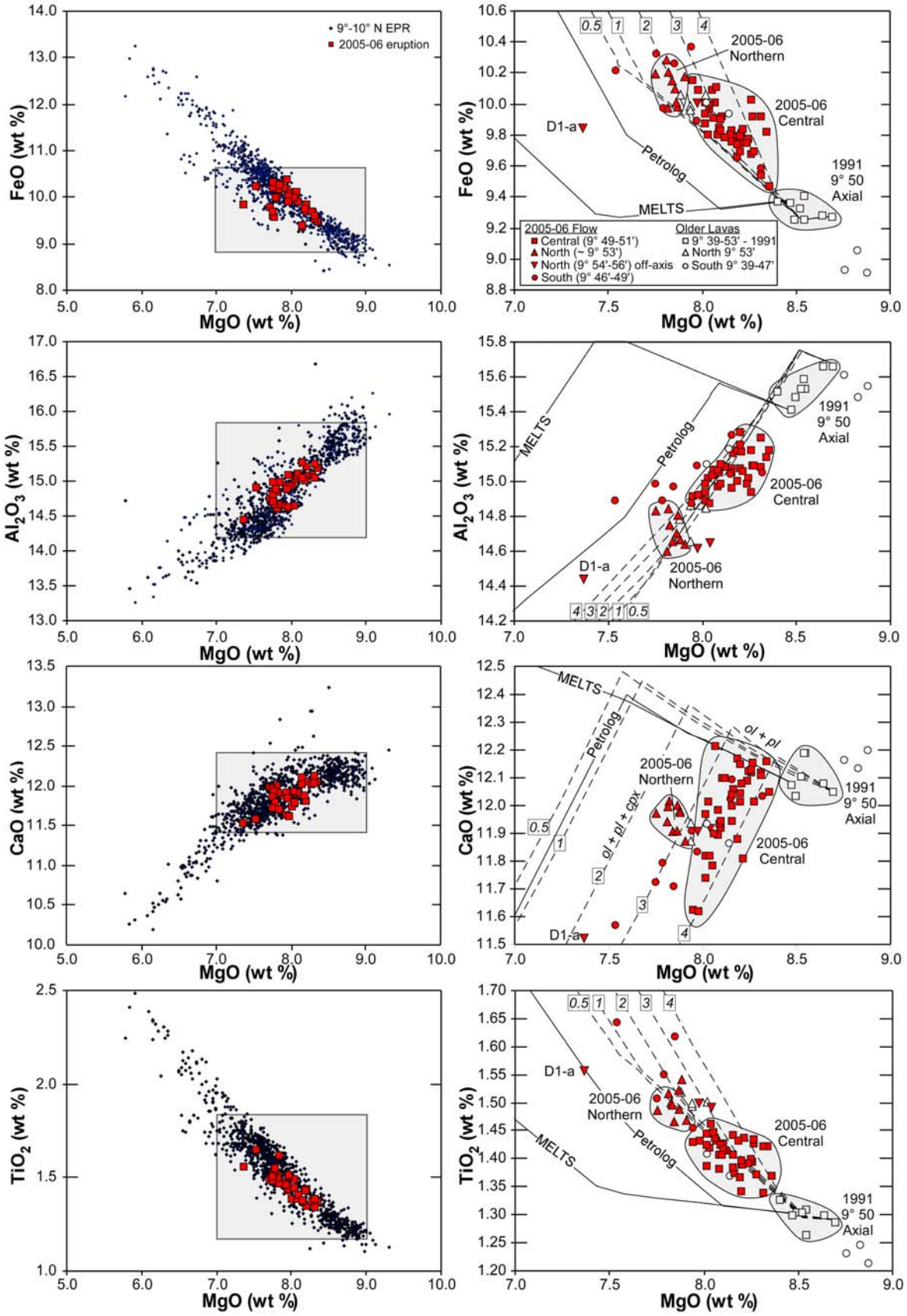
9°-10° N EPR
2005-06 eruption
FeO (wt %)
MgO (wt %)
0.5
1
2
3
4
2005-06 Northern
2005-06 Central
D1-a
Petrolog
MELTS
1991 9° 50 Axial
2005-06 Flow
Central (9° 49-51')
North (~ 9° 53')
North (9° 54'-56') off-axis
South (9° 46'-49')
Older Lavas
9° 39-53' - 1991
North 9° 53'
South 9° 39-47'
Al2O3 (wt %)
CaO (wt %)
TiO2 (wt %)
ol + pl
ol + pl + cpx

Figure 3

(Table 2). 2005–2006 central region basalts have similar, yet slightly more elevated, normalized trace element concentrations and more pronounced negative strontium anomalies than 1991–1992 EPR basalts (Figure 4). Incompatible trace element concentrations in 2005–2006 axial lavas from both the northern and southern flow regions, as well as northern off-axis lavas, are generally higher (e.g., Zr and La) than those from the central region, consistent with their more evolved major element compositions, but are similar to those from the 1992 fissure eruption near 9°53′N (Figure 4).

[17] Trace element data from both eruptions reveal clear temporal differentiation trends that are in agreement with the patterns observed in the major element data (Figure 5). 2005–2006 axial central region basalts have lower transition metal concentrations (Cr = 235–320 ppm; Ni = 85–100 ppm), higher high-field strength element (HFSE) concentrations (Zr = 85–95 ppm), and more pronounced europium anomalies (Eu/Eu* = 0.93–0.98; Table 2) compared to corresponding 1991 lavas (Cr = 304–365 ppm; Ni = 108–112 ppm, Zr < 85 ppm, Eu/Eu* = 0.99–1.08). However, Zr/Y ratios remained constant between the two eruptions (Zr/Y ~ 2.7 ± 0.1).

[18] With respect to spatial trace element patterns, all northern lavas from the last two eruptions (1992 and 2005–2006) have higher Cr concentrations at a given MgO value, and thus, fall off the main differentiation trend defined by the 1991 and 2005/2006 central region suites. Northern region lavas of both eruptions also exhibit higher Zr/Y ratios (~2.8–3.1) than those from the central region. Notably, the three northern off-axis basalts (4296-1, 4296-2, and D1-A; see Figure 2) have trace element concentrations that nearly span the entire chemical range of 2005–2006 lavas (Figure 5), yet display Zr/Y ratios like the central region lavas of both eruptions (~2.7). Off-axis sample D1-A exhibits an anomalous trace element signature with some of the lowest transition metal concentrations (Ni = 64 ppm, Cr = 247 ppm; Figure 5). Finally, trace element concentrations of axial lavas from the southern region are highly variable and include both the most and least differentiated basalts in the entire sample suite (Zr = ~103 ppm and Cr = ~220 versus Zr = ~80 ppm and Cr = ~325 ppm, respectively), despite being collected from discontinuous flows less than 100 m apart on the seafloor. Of note, the southern region axial basalts share the same Zr/Y ratios as the 1991 and 2005 axial and northern off-axis basalts (Zr/Y ~ 2.7) though the their diverse trace element concentrations do not correlate with MgO concentrations or any other chemical indicator of fractionation degree.

3.3. Radiogenic Isotopes

[19] Both axial and off-axis lavas erupted in 2005–2006 are relatively homogenous with respect to Sr, Nd, and Pb isotopic compositions (Table 3 and Figure 6). These lavas do however display some limited, but analytically resolvable, spatial and temporal Pb isotopic variability. Central region axial samples exhibit more heterogeneous Pb isotopic ratios than axial flows from the northern and southern edges of the flow field. Additionally, the off-axis fissure eruption basalts at 9°53′N yield Pb isotopic ratios that are indistinguishable from central, northern, and southern axial flows. Sr isotopic ratios range from $^{87}Sr/^{86}Sr$ = 0.70247 to 0.70251

Figure 3. Plots of major element data for samples from the 2005–2006 EPR eruption at ~9°50′N. Data are given in Table 2. (left) The 2005–2006 basalts (red squares) plotted in comparison to a compilation of ~1300 samples collected from 9°N to 10°N along the EPR (small black diamonds; from Perfit in MGDS database, http://www.marine-geo.org/tools/search/Files.php?data_set_uid=9409). (right) Complementary major element plots corresponding to the restricted compositional ranges indicated by the gray boxes in Figure 3 (left). The 2005–2006 data (red symbols) are separated into (1) northern region (filled triangles, north of 9°53′N including the Northern Arm Flow), (2) central region (squares, ~9°49′N–9°51′N), (3) southern region (circles, south of 9°49′N), and (4) northern off axis (red inverted triangles). Also plotted are older basalts (black symbols) from the 1991 BBQ flow at 9°50.5′N (squares) [*Gregg et al.*, 1996; *Perfit and Chadwick*, 1998], 1992 and older basalts from the northern region (triangles), and older oxidized flows from the southern region (circles). Dashed lines show liquid lines of decent calculated assuming fractional crystallization using the program PETROLOG [*Danyushevsky*, 2001]. Modeled liquid lines of decent (dashed lines) were calculated at pressures of 0.5 kbar, 1 kbar, 2 kbar, 3 kbar, and 4 kbar (boxed numbers) at f_{O2} = QFM using the most primitive 1991 lava (sample 2372-1) as the parental composition and assuming anhydrous conditions (H_2O = 0 wt %). Crystal-liquid equilibrium models are from *Danyushevsky* [2001]. Hydrous fractional crystallization models (H_2O = 0.2 wt %) for the 1991 BBQ flow (sample 2392-9) run with both PETROLOG and MELTS [*Ghiorso and Sack*, 1995] at 1 kbar are also shown (solid lines). These models do not reproduce the major element trends as plagioclase is suppressed early in the crystallization history resulting in higher Al_2O_3 and CaO and lower FeO and TiO_2 modeled concentrations.

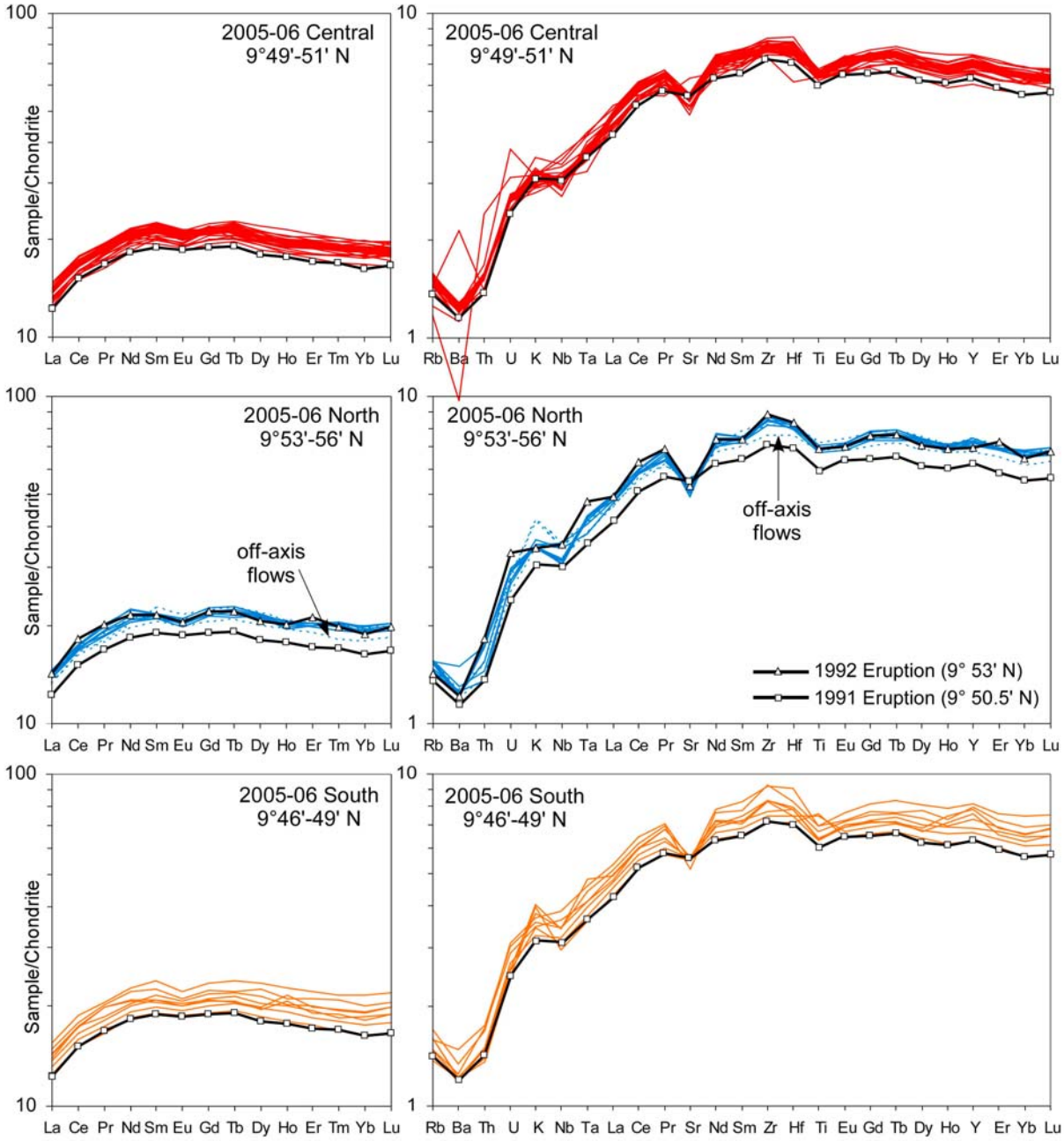

Figure 4. Chondrite normalized REE and primitive mantle normalized incompatible trace element diagrams for basalts from the 2005–006 EPR eruption at ~9°50′N. All data are given in Table 2. Normalization values are from *Sun and McDonough* [1989]. (top) Samples from the 2005–2006 central (red, 9°49′N–9°51′N) region. (middle) Samples from the 2005–2006 northern region (blue, 9°52′N–9°56′N) including those from the off-axis fissure eruption (blue dashed lines). (bottom) Samples from the 2005–2006 southern region (yellow, 9°46′N–9°50′N). Also given are the average compositions of the 1991 BBQ flow at 9°50.6′N (squares) and the separate 1992 fissure eruption at 9°53.2′N (triangles).

with an average of 0.70249 ± 0.000035 (n = 14) that is slightly less radiogenic than global average of fresh MORB (0.70280 ± 0.00027, n = 885 [*Rubin and Sinton*, 2007]) but typical of N-MORB from this region [*Sims et al.*, 2002, 2003]. The three least radiogenic samples (<0.70247) are from the central region, whereas the more radiogenic samples (>0.70250) are from the northern axial and

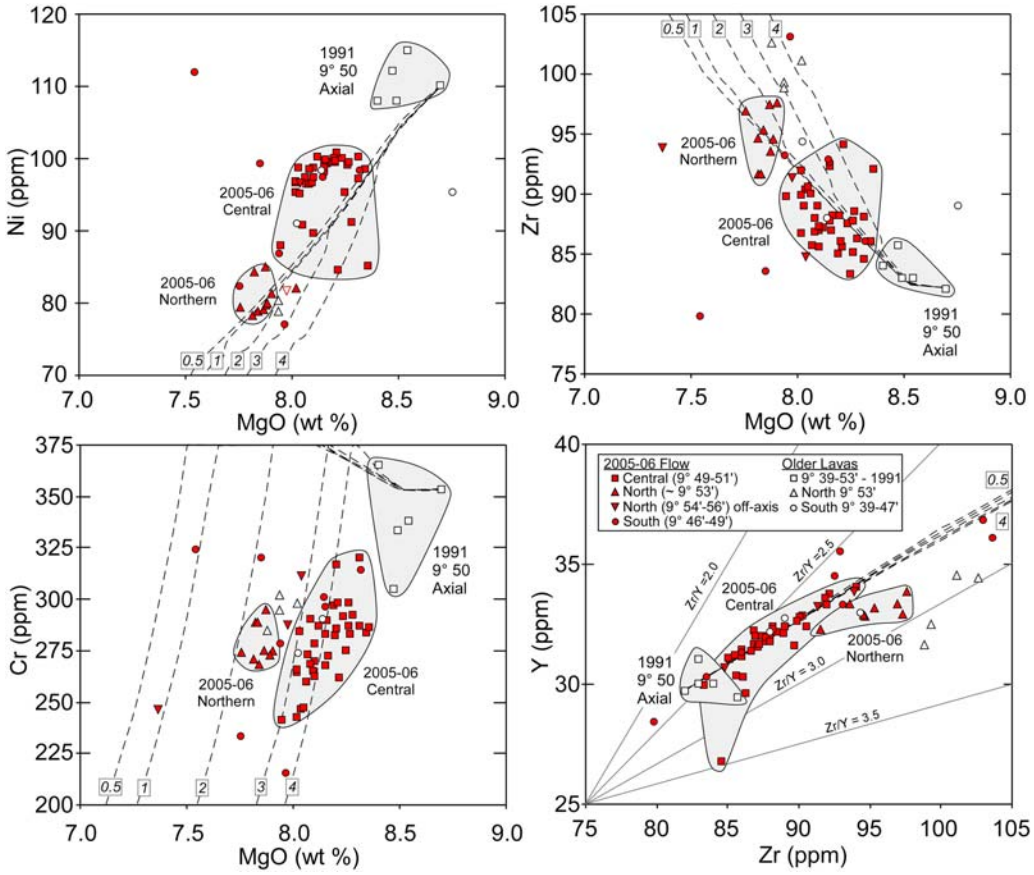

Figure 5. Trace element variation diagrams for 2005–2006 EPR basalts. Symbols are the same as in Figure 3. Dashed lines show results of Rayleigh fractionation calculations based on anhydrous fractional crystallization modeling using PETROLOG [*Danyushevsky*, 2001] for major elements. Modeled crystallization pressures and oxygen fugacity are the same as in Figure 3. Zr and Y partition coefficients (D) for olivine, clinopyroxene, and plagioclase used in the model are from *Halliday et al.* [1995] and *Dunn and Sen* [1994]. Ni and Cr partition coefficients are from *Bougault and Hekinian* [1974], with the exception of D^{ol}_{Ni} from *Nabelek* [1980].

off-axis (9°52′N–9°53′N) and southern axial (9°47′N) regions (Figure 6). Nd isotopic ratios range from $^{143}Nd/^{144}Nd$ = 0.513159 to 0.513193 (ε_{Nd} 10.2 to 10.8) with an average $^{143}Nd/^{144}Nd$ ratio of 0.513172 ± 0.000018 (ε_{Nd} = 10.39 ± 0.36; n = 14). Unlike the $^{87}Sr/^{86}Sr$ ratios, central region ε_{Nd} values fall within larger fields defined by the northern and southern regions. Despite the apparent spatial variability, mean $^{87}Sr/^{86}Sr$ and $^{143}Nd/^{144}Nd$ vary less (2σ error) than the long-term reproducibility limits defined by isotopic standard analyses (see Table 3). This suggests that all analyzed samples are isotopically indistinguishable and can be appropriately characterized by the average Sr and Nd isotopic ratios.

[20] Interestingly, a significantly older, northern axial sample (4204-3) collected from the contact of the northern 2005–2006 axial lava flow (in highly sedimented pillow terrain east of the axis) is isotopically more enriched than the 2005–2006 lavas ($^{87}Sr/^{86}Sr$ = 0.702518; ε_{Nd} = 10.2; $^{206}Pb/^{204}Pb$ = 18.314; $^{207}Pb/^{204}Pb$ = 15.478; $^{208}Pb/^{204}Pb$ = 37.733; Figure 6), even after reanalysis following stronger leaching (in 3 N HCl; see Table 3). This older sample also has distinct trace element characteristics (elevated Ba, Rb, Cs, Pb, U, and Th) with respect to 2005–2006 lavas (Table 2), and is by far the oldest-appearing sample analyzed, indicating that at least some northern region axial magma isotopic compositions were significantly different at this location prior to the 1991–1992 eruption.

4. Discussion

4.1. Mantle Source

[21] Unlike the major and trace element data, radiogenic isotope ratios from the 2005–2006 EPR

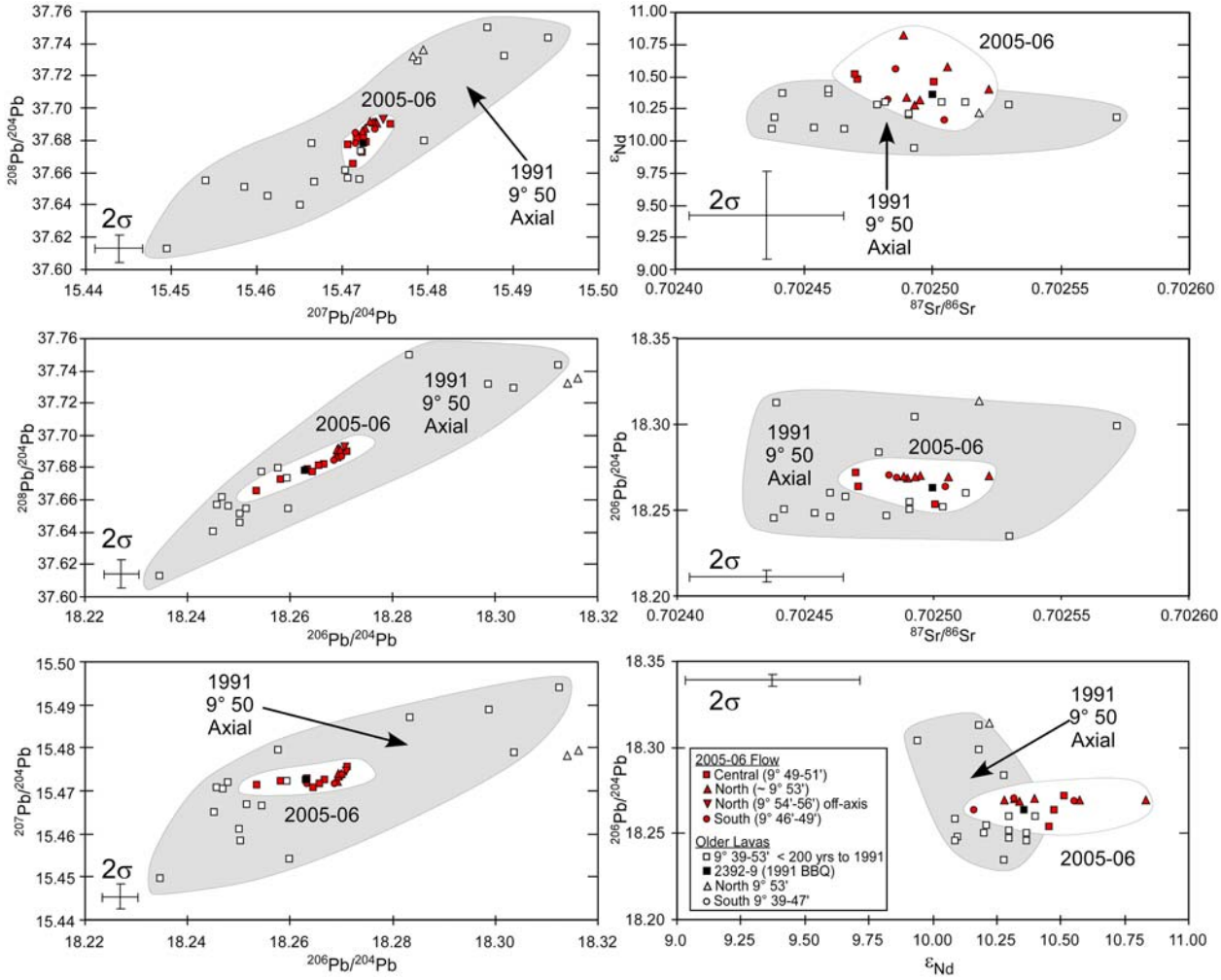

Figure 6. Sr, Nd, and Pb isotopic ratios of erupted glasses from the 2005–2006 EPR eruption. Isotopic data are given in Table 3. Symbols are the same as in Figure 3. Also plotted are older (pre-1992) axial lavas from 9°39′N to 9°53′N (open squares) [*Sims et al.*, 2002] as well as a new analysis of the 1991 BBQ flow at 9°50.6′N (2392-9, black solid square). Two Pb isotopic analyses (showing the minor analytical difference between 1N versus 3N HCl preleaching protocols (see Table 3)) and one Sr and Nd analysis of an older chemically distinct basalt (4204-3) collected in 2005 near the northern terminus of the 2005–2006 flow are represented by black open triangles. Error bars represent ±2σ reproducibility estimates determined by long-term analyses of isotopic standards.

basalts show limited spatial variation along the N-S extent of the eruption (Figure 6). The fact that all northern and southern region 2005–2006 axial basalts, as well as the off-axis basalt, have isotopic ratios identical to those from the central region suggests all 2005–2006 lavas were sourced from an isotopically homogenous mantle. This mantle composition is typical of depleted eastern Pacific mantle, showing no identifiable evidence of enriched mantle domains found on other parts of the EPR, particularly at sites of overlapping spreading centers (OSCs), transforms, and fourth-order deviations from axial linearity (or devals) [*Langmuir et al.*, 1986; *Perfit et al.*, 1994a; *Hall and Sinton*, 1996; *Sims et al.*, 2002; *Rubin and Sinton*, 2007]. Similarly, the isotopic ratios for the 2005–2006 lavas (Figure 6) fall within larger fields defined for presumably young (<~200 years, approximate age of oldest pre-1991 sample) axial lavas from 9°39′N to 9°53′N ($^{87}Sr/^{86}Sr$ = 0.70244–0.70257, ε_{Nd} +9.9 to +10.4, $^{206}Pb/^{204}Pb$ = 18.23–18.31, $^{207}Pb/^{204}Pb$ = 15.45–15.49, and $^{208}Pb/^{204}Pb$ = 37.61–37.75 [*Sims et al.*, 2002]). Thus, MORB erupted over ~20 km of ridge crest in this area have a common and fairly uniform incompatible element depleted mantle source that has been relatively constant for at least 200 years.

[22] Despite the isotopic homogeneity in the historical flows erupted at the EPR between ~9°39′N

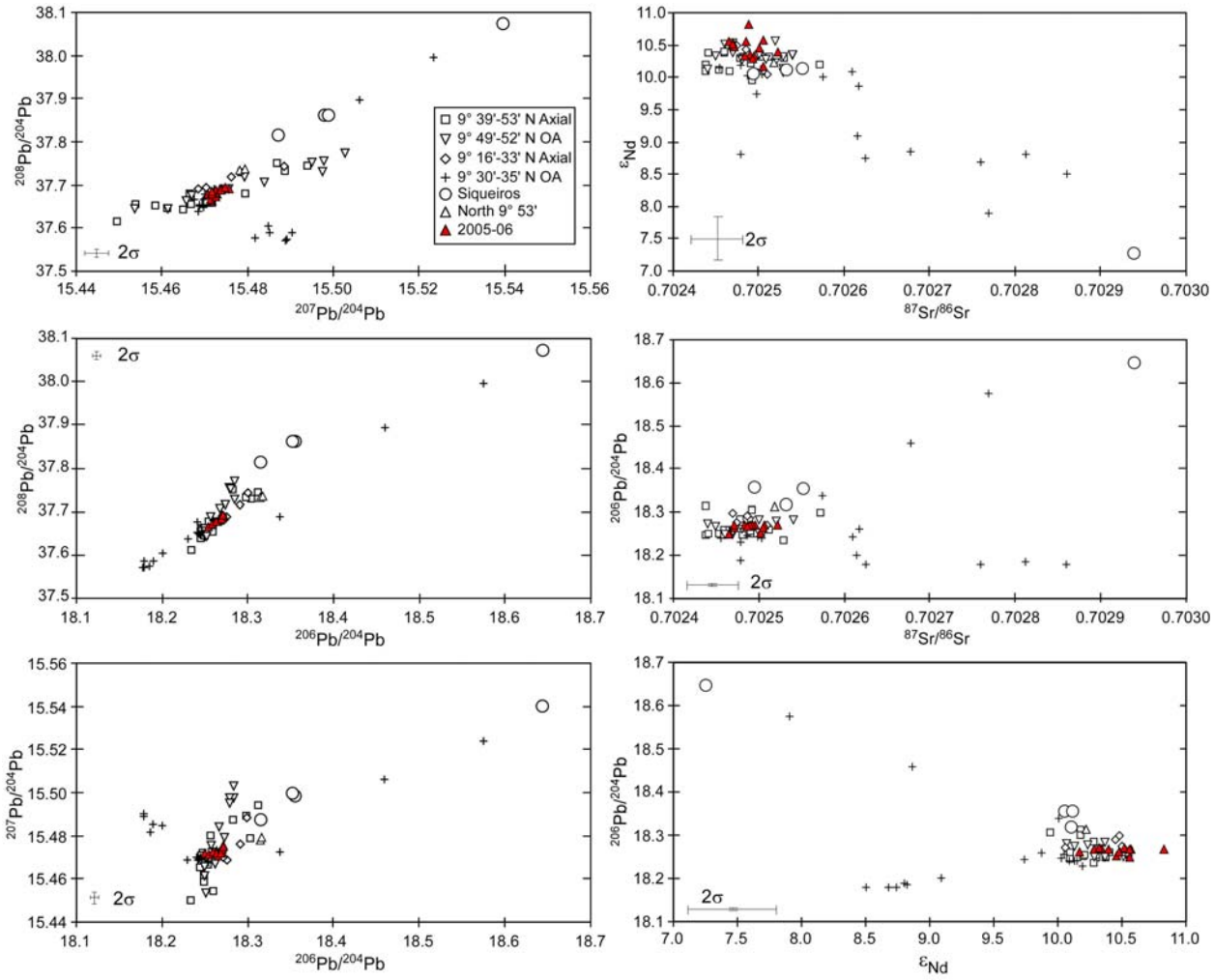

Figure 7. Sr, Nd, and Pb isotopic variations in MORB glasses from the 8°N–10°N segment of the EPR. Error bars represent ±2σ reproducibility estimates. Shown on the graph are (1) 2005–2006 EPR basalts (filled red triangles; data in Table 3), (2) older chemically distinct basalt from the northern terminus of the 2005–2006 flow (open triangles, sample 4204-3; data in Table 3), (3) young (pre-1992) axial EPR lavas from 9°39′N to 9°53′N (open squares) and 9° 16′N to 9°33′N (open diamonds) [*Sims et al.*, 2002], (4) older off-axis lavas from 9°49′N to 9°52′N (open inverted triangles) [*Sims et al.*, 2003] and 9°30′N to 9°35′N (crosses) (Waters et al., submitted manuscript, 2010), and (5) depleted (D-MORB) and enriched (E-MORB) glasses from the Siqueiros transform at 8°18′N–8°22′N (open circles) [*Sims et al.*, 2002].

and 9°56′N, there is somewhat more isotopic variability over the larger 8°N–10°N region of the EPR. For example, basalts erupted south of the 9°37′N OSC are slightly more radiogenic ($^{206}Pb/^{204}Pb$ = 18.27–18.30; $^{207}Pb/^{204}Pb$ = 15.47–15.49; $^{208}Pb/^{204}Pb$ = 37.69–37.74) than basalts from the 2005–2006 eruption (Figure 7) [*Sims et al.*, 2002]. Also, E-MORB and D-MORB from the Siqueiros Transform (8°19′N–8°22′N) and off-axis E-MORB from 9°30′N to 9°35′N have enriched isotopic values that are distinct from all other axial lavas along the 9°N–10°N segment of the EPR ($^{87}Sr/^{86}Sr$ = 0.7025–7029; ε_{Nd} +7.3 to +10.1; $^{206}Pb/^{204}Pb$ = 18.32–18.64; $^{207}Pb/^{204}Pb$ = 15.47–15.54; $^{208}Pb/^{204}Pb$ = 37.68–38.07 [*Sims et al.*, 2002; C. Waters et al., Linking asymmetric volcanic construction and temporal variations in magmatism: Evidence from isotopically enriched basalts at 9–10°N East Pacific Rise, submitted to *Journal of Petrology*, 2010]). However, off-axis E-MORB lavas from 9°30′N–9°35′N are compositionally bimodal with a subset of samples having unusually nonradiogenic Pb isotopes (see Figure 7) (Waters et al., submitted manuscript, 2010). These observations together are consistent with a model of discontinuous melt lenses separated by discrete breaks that conform to observed variations in ridge axis morphology [*Carbotte et al.*, 1998, 2000;

White et al., 2002; *Canales et al.*, 2003], such as third- or fourth-order ridge discontinuities, with each lens supplied by a mixture of melts from potentially isotopically distinct mantle sources.

4.2. Geochemical Heterogeneity Within 2005–2006 Lavas

[23] The documented compositional heterogeneity in 2005–2006 lavas provides evidence for along-axis variations in extent of melt differentiation within the oceanic lithosphere. Despite the fact that the geochemical differences among 2005–2006 lavas are small compared to larger-scale studies, major and trace element Heterogeneity Indices (HI_{ME} = 1.57 and HI_{TE} = 2.16, respectively; see *Rubin et al.* [2001] for definition and discussion) indicate significant natural geochemical differences with respect to analytical precision limits (i.e., HI > 1). This compositional variability in 2005–2006 lavas is likely to reflect petrogenetic processes operating beneath the EPR over relatively short (~10 km) spatial scales.

[24] Many of the 2005–2006 lavas from the central region have the most primitive (highest MgO wt %) and least fractionated major and trace element compositions of this eruption (Figures 3–5), suggesting that the melt within the underlying AMC in this region is comparatively hot. Furthermore, this region also appears to have erupted the largest volume of magma during the 2005–2006 eruption sequence [*Soule et al.*, 2007; *Fundis et al.*, 2008]. Together these observations suggest that the central region of the eruption is centered over what has been the most magmatically active site in the area for some time, implying that the AMC and mush zone here experience a high integrated melt input flux. This is consistent with the eruption scenario proposed by *Rubin et al.* [2008] based on ^{210}Po ages, seafloor mapping, hydrothermal vent temperature and seismicity data.

[25] Northern axial lavas have major (Figure 3) and trace element (Figure 5) compositions indicative of cooler temperatures and appear to fall along crystal fractionation paths extending from the central region lavas. Lower transition metal (Cr and Ni) and higher Zr concentrations as well as more negative Eu/Eu* anomalies (Table 2) are collectively indicative of olivine, clinopyroxene, and plagioclase fractionation. However, the compositions of the northern lavas suggest they may not be directly cogenetic with contemporaneously erupted central region magmas because of subtle compositional differences arising from slightly different melting and/or differentiation conditions (see Figure 5). Somewhat lower degrees of partial melting of the depleted mantle in this region could account for slightly higher Zr/Y ratios in northern region lavas. Higher Cr contents and CaO/Al_2O_3 ratios (Figure 8a) in northern region lavas can be produced in the crust by either a reduced or delayed onset of clinopyroxene crystallization. In sum, these differences in crystallization conditions suggest that melts within AMC are cooler in the north, perhaps because of less voluminous melt production in the underlying mantle or a less frequent supply of melt derived from the sub-AMC mush zone.

[26] Magma compositions in the southern region appear to be either slightly more differentiated versions of the common central region magma or mixtures between the central region composition and an even more evolved magma. The most primitive southern lavas geochemically resemble the most primitive central region lavas, which is consistent with either scenario. In detail, however, there appear to be two groups of southern basalts having MgO < 8.0 wt %: (1) those falling along a simple differentiation trend via fractional crystallization of central region lavas and (2) others from ~9°46′N to 9°47′N (4205-3 and 4282-1) with unusually high Cr and low Zr concentrations relative to their MgO contents that are inconsistent with simple crystal fractionation. *Smith et al.* [2001] reported axial lavas of unknown ages from the 9° 37′N OSC with 7–8 wt % MgO that likewise contain elevated Cr and lower Zr with respect to the main 9°N–10°N EPR differentiation trend. If isolated pockets of such a melt were also present at ~9°46′N, they may provide an end-member composition that could have mixed with both primary and differentiated versions of the predominant 2005–2006 magma. Mixing between compositionally heterogeneous magmas from adjacent magma chambers has similarly been reported from rift zones in Hawaii [e.g., *Garcia et al.*, 1989], Iceland [e.g., *Óskarsson et al.*, 1982], and on the southern EPR [*Sinton et al.*, 2002].

4.3. Comparison With Other 8°N–10°N Axial Lavas

[27] The occurrence of the 2005–2006 EPR eruption at the same location as fissure eruptions in 1991–1992 [*Haymon et al.*, 1993; *Rubin et al.*, 1994; *Perfit and Chadwick*, 1998; *Rubin et al.*, 2001; *Fornari et al.*, 2004], permits a direct temporal comparison between AMC melt compositions

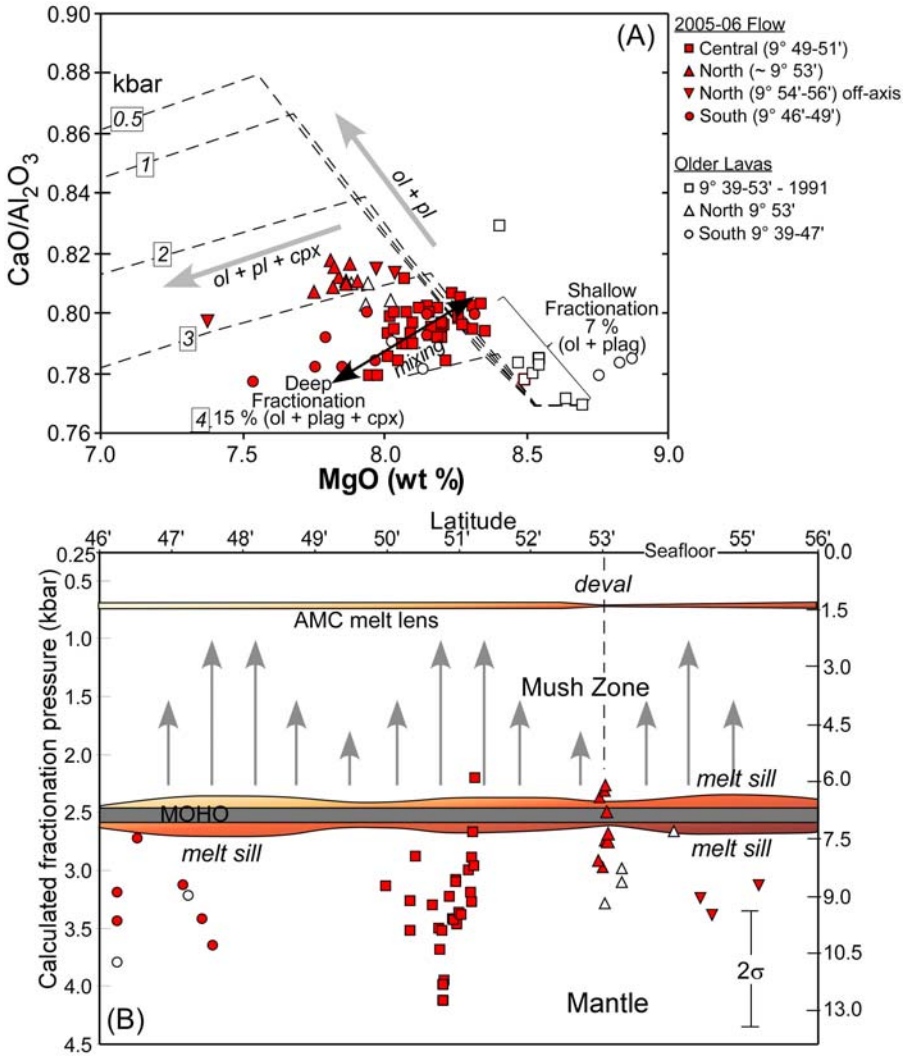

Figure 8. (a) MgO (wt %) versus CaO/Al_2O_3 for 1991–1992 and 2005–2006 lavas from the EPR at ~9°50′N. Data are given in Table 2. Symbols and parameters for fractional crystallization models are the same as in Figure 3. The abrupt inflection points in the liquid lines of decent result from the addition of clinopyroxene to the fractionation assemblage of olivine and plagioclase. At greater pressures, clinopyroxene becomes a stable phase earlier in the crystallization sequence, which is required to explain the 2005–2006 eruption geochemical trends. (b) Plot showing estimated depths of crystallization (fractionation) for the 2005–2006 EPR lavas versus latitude. Pressures (depths) are based on barometric models of *Villiger et al.* [2007] and reflect CaO-MgO equilibria for melts cosaturated in clinopyroxene and plagioclase (samples with Mg # > 0.60 were excluded due to overestimation of pressure due to olivine or olivine + plagioclase saturation in melts with Mg # > 0.60). Error estimates assuming a ~2% analytical error on major element analyses yield a 2σ pressure uncertainty of ±1 kbar [*Villiger et al.*, 2007]. AMC depth and geometry from *Harding et al.* [1993] and *Kent et al.* [1993b]. Grey vertical arrows show zones of melt upwelling through the lower crustal mush zone.

and thus provides constraints on the rates of petrogenetic processes operating within fast spreading MOR magma chambers over the time interval between eruptions. Based on the geochemical and isotopic data discussed above, melt produced during the 1991 BBQ eruption at 9°50.6′N (see Figure 2) was more primitive than, and could be parental to, the 2005–2006 magmas erupted more than a decade later. Trace element signatures of the 1991 BBQ flow [*Rubin et al.*, 1994, 2001; *Sims et al.*, 2002], including higher transition metal and lower incompatible element concentrations, combined with absent to positive Eu/Eu* anomalies and constant Zr/Y ratios are, at face value, consistent with a petrogenetic model in which the 2005–2006 magmas primarily evolved from the 1991–1992 magmas via a combination of fractional crystallization and mixing. This combination of processes

could have resulted from more than a decade of melt storage, cooling, and replenishment.

[28] In addition to the primitive 1991 BBQ flow erupted in the central region, a smaller lobate basalt flow in the north at 9°53.3′N erupted from a fissure in early 1992 (see Figure 2). Based on its more evolved geochemistry (see Figures 3–5) and younger ^{210}Po ages, *Rubin et al.* [1994] concluded that the 1992 eruption was a separate event from a different magma reservoir, possibly representing a change in magma composition from the 1991 BBQ flow. Specific defining characteristics of lavas from this region, including all other lavas erupted along this northern ridge segment over the last 2 decades, are higher Zr/Y and higher CaO/Al_2O_3 ratios (Figures 3, 5, and 8a). These observations suggest that melts stored in the crystal mush zone and/or the AMC at ~9°53′N have remained physically and compositionally distinct from central region melts for at least thirteen years, possibly because narrowing of the AMC in this region [*Kent et al.*, 1993b] inhibits flow and mixing of magmas along axis. As a result, these magmas preserve a slightly different fractionation history than the main sections of the eruption farther south. In summary, lava compositions from the 2005–2006 eruption strongly indicate that spatial compositional heterogeneity is a long-lived feature preserved over decadal time scales and relatively short spatial scales.

4.4. Petrogenetic Modeling

[29] Anhydrous fractional crystallization modeling of the most primitive 1991 lava (Figures 3 and 5, dashed lines) at f_{O2} = QFM and at various lithostatic pressures shows that major and trace element trends in the 2005–2006 basalts can be explained by fractionation of olivine, plagioclase, and clinopyroxene within the lowermost crust and/or upper mantle (2–4 kbar; 8% to up to 30% crystallization), the sub-AMC crystal mush zone (1–2 kbar; 7% to 17% crystallization), or the AMC (~1 kbar; 7% to 14% crystallization). Although near-anhydrous MORB melts can be multiply saturated at low pressure (<1–2 kbar [*Langmuir et al.*, 1990; *Grove et al.*, 1992; *Ghiorso and Sack*, 1995]), the low CaO concentrations (Figure 3), Cr contents (Figure 5), and CaO/Al_2O_3 ratios relative to those values calculated in low-pressure models (Figure 8a) suggest significant clinopyroxene crystallization early in the liquid line of decent (LLD), which occurs at higher pressures than AMC depths. In addition, hydrous fractional crystallization models (H_2O = 0.2 wt %) do not help in reproducing the observed LLDs as plagioclase crystallization is suppressed leaving olivine as the sole liquidus phase over a more extended crystallization period (Figure 3, solid lines). The composition of the primitive 1991 lava is almost certainly not representative of the most primitive melt that entered the crust from the mantle. However, its major element composition can be closely matched by 22%–24% fractional crystallization (at 2–4 kbar) of a troctolitic assemblage from a high-Mg basaltic parent like those from the Siqueiros transform fault at 8° 20′N on the EPR (2384-3; MgO = 10.12 wt %; see Figure 1 for location [*Perfit et al.*, 1996]). If this were the case, the total amount of crystallization of a gabbroic assemblage required to generate the 2005–2006 melts directly from the most primitive lavas identified on the NEPR would be increased to 25%–30%.

[30] It is well known that at moderate pressures (2–4 kbar), the clinopyroxene stability field is expanded at the expense of plagioclase and olivine [e.g., *Grove et al.*, 1992; *Elthon*, 1993], resulting in an earlier onset and greater role of clinopyroxene fractionation in controlling the LLD. Since the 2005–2006 lavas appear to require clinopyroxene fractionation, shallow level crystallization within the AMC cannot alone account for the temporal fractionation trends between 1991–1992 and 2005–2006 major/trace element compositions, suggesting that much of the differentiation between eruptions occurred deeper (i.e., at lower crustal or even possibly upper mantle depths). These models also show that as proposed above, the spatial variation in northern region Zr/Y ratios is likely controlled by melting processes within the mantle, since regardless of the modeled pressure, fractionation of a gabbroic assemblage from the 1991 melt will not substantially change the Zr/Y ratio in the resultant magma (Figure 5).

[31] Our model of deep fractional crystallization is supported by calculated crystallization pressures of 2–4 kbar estimated by Ca-Mg equilibria [*Villiger et al.*, 2007] from 2005–2006 basalt glass compositional data (Figure 8b). According to these authors, this geobarometer is sensitive to the depth of melt cosaturation in both clinopyroxene and plagioclase in MORBs with low H_2O contents (<1.0 wt %) and Mg # < 0.60. These results indicate fractionation of clinopyroxene and plagioclase from precursor melts at near-Moho depths corresponding to the lower crustal mush, mantle transition zone (MTZ), and uppermost mantle (Figure 8). It is important to note that these are maximum depth estimates with error of ± 1 kbar, and that crystallization

pressures ranging from <0.5 to 12 kbar have been previously calculated for EPR lavas from 8°N to 10°N [*Batiza and Niu*, 1992; *Villiger et al.*, 2007; *Gregg et al.*, 2009; *Natland and Dick*, 2009]. Moreover, clinopyroxene-plagioclase assemblages indicating lower crustal, MTZ, and mantle crystallization have been observed in ophiolites [*Nicolas*, 1989; *Boudier et al.*, 1996; *Kelemen et al.*, 1997; *Korenaga and Kelemen*, 1997] and exposed seafloor tectonic windows [*Hekinian et al.*, 1993], as well as proposed in other MORB suites from petrologic modeling [*Michael and Cornell*, 1998; *Natland and Dick*, 2001; *Herzberg*, 2004; *Eason and Sinton*, 2006] and experimental petrology of MORB [*Tormey et al.*, 1987; *Grove et al.*, 1992; *Kinzler and Grove*, 1992; *Elthon*, 1993; *Asimow and Ghiorso*, 1998; *Eason and Sinton*, 2006].

[32] Although clinopyroxene phenocrysts are absent in erupted 2005–2006 basalts, clinopyroxene-bearing gabbroic assemblages do occur as cumulate xenoliths found within basalts from the central region of the 2005–2006 flow (W. I. Ridley, personal communication, 2008) and from similar xenoliths from the 9°03′N OSC [*Ridley et al.*, 2008]. Crystals within these xenoliths are not in textural or compositional equilibrium with their host melts and are interpreted as fragments of the fractionated crystal-magma mush zone beneath the AMC, as was proposed for olivine anorthosite cumulates hosted in the 1991 BBQ flow [*Ridley et al.*, 2006]. It is important to note that the 1991 cumulate xenoliths contain an evolved interstitial melt (MgO = 8.0–8.3 wt %; Al_2O_3 = 15.0–15.4 wt % [*Ridley et al.*, 2006]) that is compositionally similar to 2005–2006 central region lavas with respect to many of the major elements. This indicates that such evolved melts were present in the mush zone before they were entrained by more primitive melts erupted in 1991. Similarly, interstitial melt present in 2005–2006 xenoliths is significantly more evolved (MgO = 6.0–7.0 wt %; Al_2O_3 = 15.0–13.7 (W. I. Ridley, personal communication, 2008)) than all erupted 2005–2006 lavas, suggesting further differentiation occurred within the mush zone over the last decade.

4.5. Off-Axis Volcanism

[33] In fast spreading ridge environments, axial volcanism dominates as evidenced by the prominent crestal topography, broad axial plateau and the presence of most eruptive fissures within ~500 m of the axis [e.g., *Perfit and Chadwick*, 1998]. Along the northern EPR from ~9°30′N to 9°55′N there are abundant constructional features away from the axial zone that have been mapped based on side-scan sonar data [e.g., *Fornari et al.*, 2004; *Escartín et al.*, 2007]. In addition, observations made during off-axis *Alvin* dives include the presence of glassy lava flows and pillow mounds up to ~4 km from the AST with limited sediment cover compared to surrounding presumably older flows [*Perfit et al.*, 1994a; *Macdonald et al.*, 1996; *Perfit and Chadwick*, 1998]. Some of these off-axis lavas have U-series model ages that appear to be younger than those predicted by steady state spreading rates or paleomagnetic intensity age models [*Goldstein et al.*, 1993, 1994; *Sims et al.*, 2003; *Bowles et al.*, 2006]. Moreover, profuse off-axis volcanism has been used to explain the rapid thickening of seismically imaged extrusive layer 2A within 1–4 km of the AST [*Harding et al.*, 1993; *Christeson et al.*, 1994; *Vera and Diebold*, 1994; *Christeson et al.*, 1996]. These findings have led to two end-member magmatic plumbing models to explain the apparent young off-axis volcanism. *Hooft et al.* [1996] and *Schouten et al.* [1999] proposed that all near-axial MOR volcanism originates within the AST and that infrequent voluminous lava flows [e.g., *Macdonald et al.*, 1989] overtop the AST and are transported several kilometers off-axis via surficial and/or subsurface channels [e.g., *Haymon et al.*, 1993]. These "axis-derived" flows have been reported from the 9°N–10°N, ~11°30′ N and 12°N–13°N segments of the EPR [*Hekinian et al.*, 1989; *Reynolds et al.*, 1992]. Alternatively, smaller pillow ridge lava flows emanate directly from off-axis ridge-parallel faults and fissures on the crestal plateau [*Perfit et al.*, 1994a; *Alexander and Macdonald*, 1996; *Macdonald et al.*, 1996; *Perfit and Chadwick*, 1998; *Reynolds and Langmuir*, 2000; *White et al.*, 2002]. Here we discuss the geochemical and isotopic signature of a confirmed off-axis fissure eruption in light of the existing structural models above for off-axis magmatism at MORs.

[34] Previous studies have examined the geochemistry of lavas collected off axis [*Sims et al.*, 2003; Waters et al., submitted manuscript, 2010], although the original eruption location and age of these flows is unknown. Generally, off-axis ridge lavas are chemically distinct from axial and "axis-derived" off-axis flows, having more evolved compositions that are petrogenetically related to more primitive axial lavas via fractional crystallization or with chemical characteristics indicating derivation from E-MORB parental magmas [*Perfit et al.*, 1994a; *Sims et al.*, 2003]. However, our data agree with those presented by *Sims et al.* [2003] for

a suite of off-axis pillow mounds at 9°52′N with anomalously young U-Th and Th-Ra model ages and radiogenic Sr, Nd, and Pb isotopes that are identical to nearby axial lavas.

[35] The 2005–2006 off-axis lavas from 9°53.3′N to 9°56.4′N also underwent greater extents of magmatic differentiation than most axial 2005–2006 lavas from the central region, although perhaps nonintuitively, they are slightly less differentiated than northern axial lavas. Trends in the major and trace element data suggest mixing may have occurred between the strongly differentiated northern and more primitive central region magmas. However, the northernmost off-axis ^{210}Po-dated dredged basalt from 9°54.5′N (D1-A (K. H. Rubin, personal communication, 2008)) has anomalous major and trace element signatures and is unlikely to be directly petrogenetically related to any of the other lavas erupted in 2005–2006.

[36] Given the narrow half-width (~350 m) of the AMC at ~9°50′N [*Kent et al.*, 1993b], the eruption of fractionated off-axis lavas was likely restricted to a narrow region corresponding to zones of active faulting as initially proposed by *Carbotte et al.* [1997]. Considering an average AMC depth of ~1.4 km and thickness of ~50 m [*Harding et al.*, 1993; *Kent et al.*, 1993b], an axis-dipping normal fault like the inward dipping normal fault that bounds the off-axis flow to the east, would require a maximum dip of ~80° to intersect the cooler edges of the AMC. Such axis-parallel faults (Figures 1 and 2) are geophysically well documented for the 9°N–10°N segment of the EPR [*Fornari et al.*, 1998, 2004; *Escartín et al.*, 2007] and provide pathways to facilitate diking that may have fed the off-axis fissure lava flow at 9°53′N–9°56′N. Alternatively, syneruptive movement on the near-axis normal fault may have modified the local stress field and caused the intruding dike to deflect away from the ridge axis. Finally, the off-axis eruptions could have been sourced from a small isolated off-axis melt lens. Though recent 3-D seismic imaging studies have identified off-axis melt lenses, they are ~4–7 km east of the ridge axis at 9°54′N, considerably east of the off-axis fissure eruption [*Canales et al.*, 2008; *Carbotte et al.*, 2008]. In any event, our geochemical data do not require a completely independent off-axis plumbing system with isolated and spatially restricted evolved magma bodies, as has been proposed for other fault-bound off-axis eruptions [e.g., *Goldstein et al.*, 1994; *Perfit et al.*, 1994a].

4.6. Short-Term Small-Scale Magmatic Processes at Fast Spreading MOR

[37] The observed small-scale spatial geochemical heterogeneity in 2005–2006 EPR basalts places additional constraints on the structure, segmentation, and interconnectivity of melt below the ~9°50′N segment of the EPR. Between the Clipperton Fracture Zone and 9°17′N deval (Figure 1), geophysical imaging has revealed what appears to be a continuous "boudinage-shaped" AMC measuring ~700 m wide and 10–50 m thick [*Detrick et al.*, 1987; *Kent et al.*, 1990, 1993b] ~1.4 km below the AST [*Harding et al.*, 1993]. This sill-like AMC along the 9°N–10°N EPR coalesces into a "melt lens" below the active neovolcanic zone (see Figure 9) [*Perfit and Chadwick*, 1998]. In detail, the AMC between 9°17′N and the Clipperton FZ is segmented, with tapered AMC widths at the 9°17′N and 9°53′N devals, and at a small OSC at 9°35′N [*Kent et al.*, 1993b; *Smith et al.*, 2001]. Narrow "pinch outs" at these devals and OSCs may restrict along-axis magma mixing between tectonically segmented melt lenses each measuring ~30 km along the axis [*Morton et al.*, 1987; *Harding et al.*, 1989].

[38] This concept of thin disconnected melt reservoirs along the EPR is supported by the spatially heterogeneous geochemical data. As previously shown [*Langmuir et al.*, 1986; *Sinton et al.*, 1991], petrologically similar lavas erupt from chemically distinct AMCs separated by devals, with each lens supplied independently from the mantle source via the lower crust. *Langmuir et al.* [1986] explained the confinement of enriched T-MORB ("transitional") magmas to ridge discontinuity boundaries as a result of a compositionally heterogeneous mantle and/or lower melting percentages at these locations. They proposed that spatial compartmentalization of various AMCs inhibited complete and efficient mixing between compositionally distinct mantle melts. Our data support this model, as both 1992 and 2005 lavas that erupted north of the 9°53′N deval are markedly different and suggest different extents of melting (e.g., higher Zr/Y) and shallower fractionation histories than lavas erupted in the central region during both eruptions.

[39] Furthermore, recent 3-D seismic and tomographic imaging of the 9°30′N–9°50′N region show that AMC segmentation is evident at even smaller (~5 to 10 km) spatial scales [*Toomey et al.*, 1990; *Carbotte et al.*, 2008, 2009] and ≤1 km–scale geochemical variability has been reported for

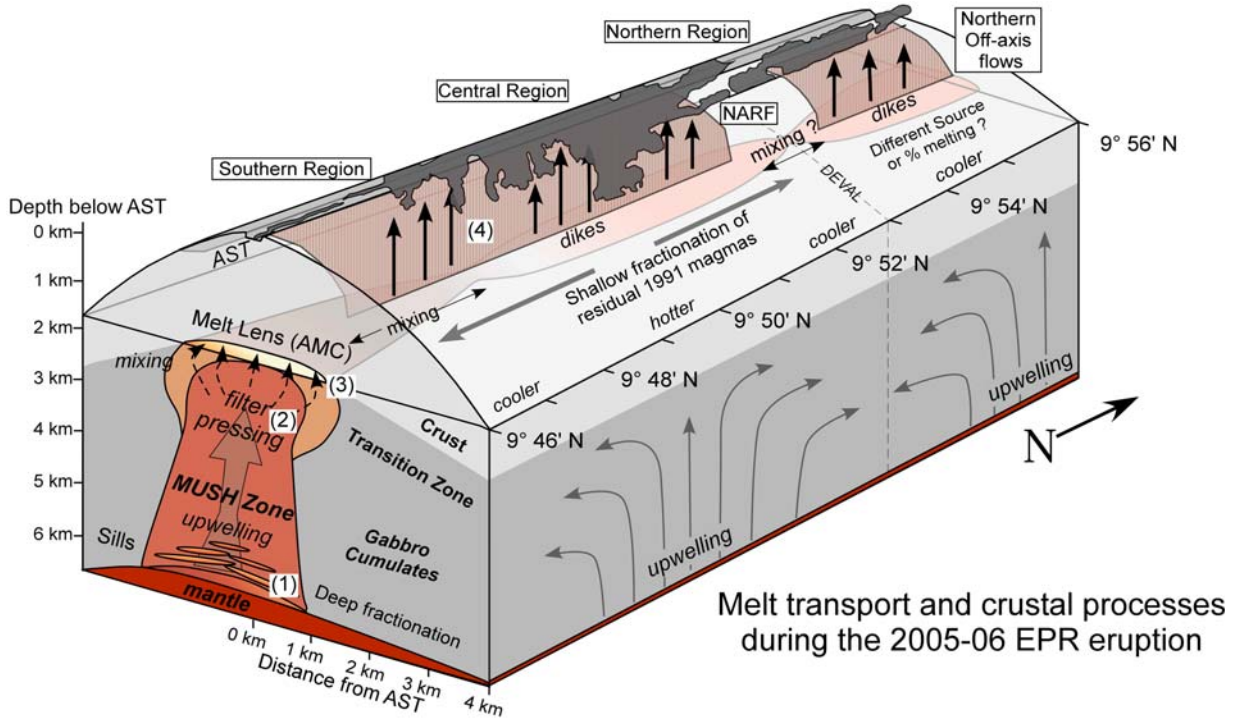

Figure 9. Three-dimensional representation of the 9°46′N–9°56′N segment of the EPR showing principle tectonic features and magmatic model. Outline of the 2005–2006 eruption is modified from *Soule et al.* [2007]. Dashed line shows location of the 9°53′N deval. The wide arrow (front) and gray near-vertical arrows (side) show directions of upwelling melt moving from lower crustal sills (indicated by 1), percolating through the crystal mush zone (indicated by 2), filter pressed into (dashed arrows) and ultimately stored within the AMC (indicated by 3), and finally erupted via near-vertical dikes to the surface (indicated by 4). Grey horizontal arrows show along-AMC crystal fractionation trends determined from the geochemical data. NARF, northern arm flow. Grey arrows shown on the side depict two possible melt upwelling cells beneath the axial summit trough (AST) separated by the 9°53′N deval.

extensive lava fields along other segments of the EPR [*Perfit et al.*, 1994a; *Hall and Sinton*, 1996; *Smith et al.*, 2001; *Castillo et al.*, 2002; *Sinton et al.*, 2002; *Bergmanis et al.*, 2007; *Geshi et al.*, 2007], the Juan de Fuca Ridge [*Embley et al.*, 2000; *Stakes et al.*, 2006], the Mid-Atlantic Ridge [*Machado et al.*, 1982], and on Iceland [*Maclennan et al.*, 2003]. These studies challenge the view that individual ocean ridge magma chambers effectively homogenize magma injected from compositionally variable parts of the mantle [e.g., *Fornari et al.*, 1988; *Sinton and Detrick*, 1992; *Niu and Batiza*, 1997] and indicate that this heterogeneity can be petrologically evident in a suite of lavas from one eruption, particularly if sampled with sufficient density [e.g., *Rubin et al.*, 2009]. As discussed by *Sinton and Detrick* [1992], AMCs with extremely low aspect ratios (h/w = ~0.01 to 0.07) such as observed on the EPR, would be expected to have strongly spatially limited convection. This would limit physical mixing and in turn result in a geochemically heterogeneous AMC; evidenced by 2005–2006 basalts erupted in the southern and central regions that exhibit discernable compositional variations (Figures 3–5). The geochemical variability in central region lavas alone indicates incomplete mixing of parental magmas, despite the presumably high melt supply inferred by the frequent and focused magmatism and high-temperature hydrothermal activity in the 9°50′N EPR region.

[40] At the base of the AMC is a diffuse low-velocity region extending up to 4 km off axis [*Toomey et al.*, 1990; *Vera et al.*, 1990] that has been attributed to a partially molten crystal mush zone containing between 2.5% and 18% melt [e.g., *Caress et al.*, 1992; *Sinton and Detrick*, 1992; *Key and Constable*, 2002] (see Figure 9). Phase chemical studies of an ol-anorthositic gabbroic xenolith from the 1991 BBQ flow show that incomplete melt homogenization is also evident in this zone on

centimeter scales [*Ridley et al.*, 2006]. Sandwiched between the crystal mush and underlying mantle, sill-like melt bodies within the gabbroic lower crust have been (1) imaged using geophysical techniques [*Garmany*, 1989; *Crawford et al.*, 1999; *Crawford and Webb*, 2002; *Key and Constable*, 2002; *Canales et al.*, 2009], (2) exposed as plutonic sections in dismembered "tectonic windows" along the EPR [*Francheteau et al.*, 1990; *MacLeod et al.*, 1996; *Karson et al.*, 2002], and (3) interpreted from observations within the lower crustal and mantle sections of the Oman ophiolite [*Boudier et al.*, 1996; *Kelemen et al.*, 1997].

[41] Given that our geochemical data indicate a role for moderately high pressure crystallization within the lower crust and/or uppermost mantle (2–4 kbar; Figure 8), transport of differentiated melt from lower crustal sills, through the mush zone to the AMC via continual percolation or channel flow must have also occurred on a relatively rapid, roughly decadal time scale. Assuming a melt lens with dimensions similar to the 9°50′N AMC (h = 50 m, w = 350 m), a latent heat of crystallization of 500 kJ/kg, an average density of 2700 kg/m^3, and a hydrothermal power output of 160 MW per km along the ridge [*Ramondenc et al.*, 2006], complete crystallization of the AMC would occur within ~4.6 years. Therefore, melt replenishment of the AMC would have been required to prevent the melt lens from completely freezing during the repose period (1992–2005). Similarly, recent thermal modeling by *Liu and Lowell* [2009] shows that decadal-scale magma replenishment of similar sized AMCs is required to maintain the observed steady focused flow vent temperatures (>250°C) reported at 9°50′N from 1991 to 2005 [*Von Damm*, 2004; *Scheirer et al.*, 2006]. Specific to the 9°50′N region, fractionated melt at the base of the lower crust at ~6 km depth [e.g., *Natland and Dick*, 2009] would have to vertically migrate through a mush column at ~380 m/yr or ~1 m/d to reach the AMC following the 1991–1992 eruption. These rapid melt migration rates are somewhat faster than those reported by *Liu and Lowell* [2009] (3–30 m/yr) yet generally agree with crustal residence times for 1991–1992 EPR magmas calculated from ^{210}Pb-^{226}Ra-^{230}Th disequilibria in young MORB [*Rubin et al.*, 2005].

[42] Although there is no direct geochemical evidence for the existence of magma significantly more primitive than the 1991 BBQ flow, or for one greatly more evolved than the 2005–2006 lavas in the crust, it is highly probable that some degree of mixing of compositionally variable precursor melts occurred within the AMC before the most recent eruption. Any existing magmas resident in the AMC in 1991–1992 could only have evolved at low pressures (~1 kbar) despite the above models that require fractional crystallization at various depths within the subridge crust and mantle. Therefore, we suggest that residual 1991–1992 BBQ magma evolved via low-pressure fractional crystallization before mixing with variable amounts of ascending evolved melt that was leaking into the AMC from deeper levels within the mush zone [e.g., *Natland and Dick*, 2009]. In this model, the amount of added melt needed to "refill" the AMC would depend on how much fractional crystallization occurred in the AMC since 1991. At these shallow depths, only ~5%–10% fractional crystallization of a troctolitic (olivine + plagioclase) assemblage would change the composition of residual 1991–1992 magmas to those like the most primitive central region lavas from 2005 to 2006 (Figures 3 and 8a). We conclude that following the 1991–1992 eruption, there likely was a variety of fractionated melts that eventually accumulated in the AMC where they mixed to different extents to generate the composite compositions found in the 2005–2006 erupted lavas.

4.7. Mechanisms Driving Eruptions Along the EPR

[43] Despite a half century of mid-ocean ridge scientific study, few direct observations and data exist regarding the physical mechanisms that cause new MOR eruptions, primarily due to the general lack of in situ temporal observations. The interplay between preeruptive and syneruptive seismicity, magma chamber processes, diking/cracking, and hydrothermal activity have up to this point largely been addressed by studies at the CoAxial segment [*Embley et al.*, 2000] and Axial seamount [*Chadwick et al.*, 1999; *Nooner and Chadwick*, 2009] along the Juan de Fuca ridge and along nonactive ridge segments of the EPR [e.g., *Carbotte et al.*, 1998]. Unlike these studies however, the 2005–2006 EPR eruption provides an opportunity to examine the modern physical state of the AMC with respect to past conditions, and to discern how the system has changed over a decadal time scale.

[44] Our data indicate that the 2005–2006 lavas reflect differentiated and mixed residual melts derived from more primitive 1991–1992 basaltic magmas. Based on this conclusion, no geochemical evidence exists to indicate the 2005–2006 EPR

eruption was catalyzed by an injection of hotter more primitive melt into a cooling and crystallizing magma chamber, as is generally presumed and often proposed for compositionally mixed magma chambers in convergent and intraplate margins [e.g., *Wright*, 1973; *Sparks et al.*, 1977; *Garcia et al.*, 2000; *Goss et al.*, 2009]. As proposed above, more evolved residual magmas stored in the subaxial crystal mush zone following the 1991 eruption likely incrementally replenished the AMC over a decadal period (Figure 9), leading to crustal dilation, magmatic overpressurization, and eventual eruption in mid-2005. Such a filter-pressing or synkinematic differentiation model [e.g., *Natland and Dick*, 2001; *Gao et al.*, 2007], where the weight of settling crystals within the mush zone results in the expulsion/squeezing of fractionated liquids into the base of the AMC, has been proposed for layered mafic intrusions [*McBirney*, 1995; *Tegner et al.*, 2009], MOR [*MacLeod et al.*, 1996; *Faure and Schianoa*, 2004], and lava lakes in Hawaii [*Wright and Okamura*, 1977].

[45] In addition to AMC overpressure, we propose that extensional forces, both local and external to the local ridge axis, facilitated the eruption. The local tensional stresses applied to the ridge generate sporadic pulses of extension focused along or near the ridge axis [e.g., *Buck et al.*, 2005]. Also, extension and normal faulting may have been generated locally by thermal stresses from hydrothermal cooling [*Sohn et al.*, 1999; *Wilcock et al.*, 2002; *Sohn et al.*, 2004] or by magma intrusion [e.g., *Rubin*, 1992]. The latter mechanism has been invoked by *Wilcock et al.* [2009] to explain the observed microseismicity patterns and focal mechanism distribution along the Endeavor segment of the Juan de Fuca Ridge. These authors further find that sustained injection of magma into the AMC would be required to maintain the observed stress field given passive degassing along the ridge axis; which agrees with our proposed model for the 2005–2006 eruption. In addition to local tensional forces, the tectonic "slab pull" force [*Spence*, 1987; *Conrad and Lithgow-Bertelloni*, 2002] exerted on the ridge, ultimately derived from the subduction of dense EPR-derived lithosphere, may further contribute to the extensional strain facilitating magma ascent. These applied tensional forces strained the EPR crust, aiding preeruption cracking/diking that lasted for 1.5 years as observed by the gradual ramp up in microseismicity recorded by OBS reported by *Tolstoy et al.* [2006]. How much of this preeruption microseismicity is driven by extensional forces versus tumescence of an overpressurized magma chamber and/or cracking due to magma ascent remains unknown. At some point however, deep axis-parallel fractures, possibly reactivating preexisting weaknesses associated with the 1991–1992 eruption, eventually intersected and decompressed the AMC, permitting the fractionated melt to incompletely degas [e.g., *Michael et al.*, 2008] as it rose rapidly to the surface along the ridge.

[46] The strong negative correlation between eruption interval along MORs and full spreading rate predicts that fast spreading centers such as the 9°N–10°N EPR should erupt on annual to decadal time scales [*Perfit and Chadwick*, 1998; *Rubin and Sinton*, 2007]. The 13 year hiatus between the 1991 and 2005–2006 EPR eruption is consistent with this hypothesis. Such eruptive cyclicity is not driven necessarily by the rate in which primitive mantle-derived melt can ascend and fill a deflated AMC, but rather by the rate in which forces acting on the ridge locally depressurize an AMC continuously replenished by compositionally diverse melts from the underlying crystal mush. Over time, and possibly on greater than decadal time scales, we suggest that primitive melt from the underlying depleted mantle repopulates the crystal mush zone to fully complete the magmatic cycle.

5. Conclusions

[47] This study marks the first investigation of the geochemistry and petrology of the 2005–2006 EPR eruption at ~9°50′N: the best documented repeat eruption along the global MOR system. The main conclusions are as follows:

[48] 1. The 2005–2006 lavas exhibit limited spatial compositional variability, most of which is inherited during differentiation within the crust and/or uppermost mantle. New lavas erupted in the central region are the most primitive, whereas those on the northern limits are more evolved and may have been physically separated from the main magma source. Southern region flows are geochemically heterogeneous and include lavas with the lowest MgO. Cooler magmas from the northern and southern distal edges of the eruption suggest either more subdued magma input or enhanced cooling rates in the AMC in these locations.

[49] 2. Lavas erupted off axis in the northern region are geochemically similar to nearby axial lavas, however both may contain a small component of melt derived from smaller degrees of mantle partial melting and/or a different crystallization history.

[50] 3. Radiogenic isotope ratios of all 2005–2006 basalts show little spatial heterogeneity and are identical to those from the 1991–1992 basalts. This indicates that the entire 2005–2006 eruption, as well as the smaller 1991–1992 eruption, was fed by melts derived from a common depleted mantle source.

[51] 4. The 2005–2006 basalts are more differentiated than those from the 1991–1992 eruptions from the same locations. However, spatial geochemical differences apparent in both eruptions are persistent long-lived features associated with the morphology and connectivity of the subaxial melt lenses. Geochemical trends and fractional crystallization modeling show that the 2005–2006 basalts most likely are residual fractionated liquids remaining after the 1991–1992 eruptions that have been mixed with more evolved magmas from deeper in the crust. Calculated liquid lines of decent coupled with estimates of crystallization depth suggest some component from melts that crystallized within lower crustal melt sills (2–4 kbar) that incompletely mixed with various melts within the shallower crust or AMC.

[52] 5. A model of progressive AMC replenishment would ultimately prevent the complete solidification of the melt lens over the 13 year repose period and is supported by heat balance calculations that require a semicontinuous supply of melt to the AMC from the crystal mush zone.

[53] 6. The 2005–2006 eruption was likely triggered by overpressure caused by incremental percolation of fractionated liquids from the mush zone into the AMC, not by the injection of hotter more primitive magma into the AMC.

Appendix A: Geochemical Methods

A1. Major Elements

[54] Major elements were analyzed using a JEOL 8900 Electron Microprobe on polished glass chips at the USGS Microbeam Laboratory in Denver (CO) using standard minerals for elemental calibrations and a full ZAF matrix correction. Average analyses of seven to ten separate points for each sample were normalized and corrected for instrument drift based on the established values for in-house standards JdF-D2 and ALV2392-9 [see *Smith et al.,* 2001]. Elemental external reproducibility (2σ) calculated from variation in the analyses of ALV2392-9 during these analytical runs and repeat analysis of previously analyzed glasses is generally <1%–3% (see Table 2) except MnO, K_2O, and P_2O_5 that can have appreciably higher error where concentrations are low (<0.2 wt %).

A2. Trace Elements

[55] Macroscopically fresh fragments (1–5 mm diameter) of natural glass chipped from quenched lava crusts were handpicked using a stereoscope avoiding phenocrysts, microlites, and rare heavily MnO-encrusted and/or altered fragments. Glasses were subsequently cleaned ultrasonically for 5–7 min in a 60:40 solution of 1.4 N HCl (trace metal grade) and 30% H_2O_2. After ensonification, approximately 50 mg of the cleanest glass chips were handpicked and placed in 7 ml Teflon Savillex© hexavials that had been precleaned for 24 h each with 14 N NHO_3 and 14 N HCl, followed by 24 h sequential hotplate reflux in Optima grade 6 N HCl. Vessels were washed between cleaning stages with 4x quartz distilled deionized H_2O. Glass chips were digested with 1 mL of concentrated HF + 2 mL of concentrated HNO_3 for 48 h at 100°C, dried down, refluxed overnight with 1 mL of 6 HCl to convert insoluble fluorides to chlorides and then evaporated to a soluble residue. Optima grade acids were used in all leaching, digestion, and analytical procedures. Residues were diluted with ~4.5 mL of 5% HNO_3 + 100 ppm HF spiked with 8 ppb each of Re and Rh, capped and refluxed on a hotplate overnight. A procedural blank was prepared with each batch of samples to monitor acid purity and environmental contamination. Unknowns were diluted 2000x and analyzed in medium resolution mode for 34 trace elements on a high-resolution magnetic sector Element2 Inductively Coupled Plasma Mass Spectrometer (ICP-MS) at the University of Florida, Department of Geological Sciences. Re and Rh were used as internal standards to correct for instrumental drift and matrix effects. Blanks were subtracted from the count totals, and data quantified by external calibration using a combination of USGS (AGV-1, BIR-1, BHVO-1, BCR-1) and internal (Endeavor Ridge (ENDV) MORB standard from the Geological Survey of Canada, Ottawa) rock standards. Instrumental drift, as well as data accuracy and long-term reproducibility were assessed by sequential analyses ($n = 9$) of a secondary internal standard, ALV2392-9. External long-term reproducibility is <3% for most trace elements except for those with extremely low concentrations in MORB lavas including Rb (6%), Ba (5%), Ta (6%) Pb (19%), and U (5%).

Table B1a. Comparison of New Pb Isotopic Data With Published Values[a]

	UF		ENS Lyon		UF		ENS Lyon		UF		ENS Lyon	
	$^{208}Pb/^{204}Pb$	2σ	$^{208}Pb/^{204}Pb$	2σ	$^{207}Pb/^{204}Pb$	2σ	$^{207}Pb/^{204}Pb$	2σ	$^{206}Pb/^{204}Pb$	2σ	$^{206}Pb/^{204}Pb$	2σ
2384-3	37.823	0.0090	37.861	0.0095	15.489	0.0028	15.499	0.0054	18.325	0.0034	18.353	0.0064
2752-6	37.699	0.0090	37.743	0.0094	15.477	0.0028	15.494	0.0054	18.287	0.0034	18.313	0.0064
2392-9	37.667	0.0090	37.612	0.0094	15.472	0.0028	15.450	0.0054	18.247	0.0034	18.235	0.0064
2392-9	37.678	0.0086			15.472	0.0028			18.264	0.0034		
2392-9	37.682	0.0086			15.473	0.0028			18.265	0.0034		
2392-9	37.677	0.0086			15.471	0.0028			18.263	0.0034		
2392-9	37.678	0.0086			15.472	0.0028			18.263	0.0034		
2390-5b	38.071	0.0086	38.073	0.0095	15.538	0.0028	15.540	0.0054	18.643	0.0034	18.645	0.0065
2390-5b	38.072	0.0086			15.538	0.0028			18.644	0.0034		
2390-5b	38.076	0.0086			15.540	0.0028			18.645	0.0034		
2390-5	38.077	0.0086			15.540	0.0028			18.646	0.0034		
2759-14	37.677	0.0090	37.729	0.0094	15.472	0.0028	15.498	0.0054	18.210	0.0034	18.284	0.0064
2759-14	37.679	0.0086			15.471	0.0028			18.260	0.0034		
D20-2	37.841	0.0086	37.861	0.0095	15.490	0.0028	15.498	0.0054	18.340	0.0034	18.355	0.0064
2703-1	38.004	0.0086	37.997	0.0095	15.525	0.0028	15.524	0.0054	18.576	0.0034	18.574	0.0065

[a]*Sims et al.* [2002, 2003]. Bold numbers indicate analyses run in February 2008; other analyses run in April 2008. Precision estimates (2σ) reflect long-term analyses (n = 40) of Pb standard NBS 981 and are $^{206}Pb/^{204}Pb$ = ~206 ppm, $^{207}Pb/^{204}Pb$ = ~194 ppm, and $^{208}Pb/^{204}Pb$ = ~238 ppm. Reproducibility for published data is $^{206}Pb/^{204}Pb$ = ~350 ppm, $^{207}Pb/^{204}Pb$ = ~350 ppm, and $^{208}Pb/^{204}Pb$ = ~250 ppm [*Sims et al.*, 2002, 2003].

A3. Radiogenic Isotopes

[56] Cleaned glass chips (~100 mg) selected for isotopic analyses were leached a second time in 1 N HCl + 2% H_2O_2 and then twice in 4x QD H_2O to remove any secondary handling contamination and residual alteration. Leached glasses were dried and then digested in 3 ml HNO_3 + 1.5 ml HF, evaporated to dryness, refluxed for 24 h in 6 N HCl and then evaporated to a residue. All chromatographic elemental separations were performed within a class 1000 clean laboratory equipped with class 10 laminar flow hoods at the University of Florida. Pb was separated from the dissolved sample through 100 μl Teflon columns packed with Dowex© AG1X-8 anion exchange resin (100–200 mesh) using standard anion exchange techniques in HBr eluent. The sample was washed 3x with 1 mL 1 N HBr and the Pb fraction was collected in 1 mL 3N HNO_3. The 1N HBr was collected for subsequent Sr and Nd separation, as both elements are not absorbed on the Dowex resin. Sr and Nd were further purified for isotopic analysis following standard chromatographic methods. Biorad AG50W resin columns were used to separate Sr from the REE. Secondary purification of the Sr fraction was achieved by eluting the Sr separate through 100 μl Teflon columns packed with Eichrom Sr Spec© resin. Nd was separated from the REE fraction via elution through 100 ml columns of HDEHP-coated resin following methods adapted from *Pin* [1997].

[57] All samples were analyzed for Sr, Nd, and Pb isotopes on the Nu-Plasma© multicollector (MC) ICP-MS at the University of Florida. Analyte fractions were diluted in 2% HNO_3 and aspirated into the plasma via a DSN-100 desolvation nebulizer to achieve ~2–8 V of total ion current at 5–15 pbb solution concentrations. Pb isotopic measurements were run in static traditional mode composed of 3 blocks of 15 analyses each, with zero background signal measured off peak at the start of each run and between separate blocks. Pb

Table B1b. Comparison of New Sr and Nd Isotopic Data With Published Values[a]

	UF		WHOI		UF		UC-Berkeley	
	$^{87}Sr/^{86}Sr$	2σ	$^{87}Sr/^{86}Sr$	2σ	ε_{Nd}	2σ	ε_{Nd}[b]	2σ
2384-3	0.702551	0.00003	0.70255	0.00006	9.9	0.34	10.1	0.20
2752-6	0.702486	0.00003	0.70244	0.00005	10.7	0.34	10.2	0.20
2392-9	0.702500	0.00003	0.70253	0.00003	10.4	0.34	10.3	0.20
2759-14	0.702501	0.00003	0.70250	0.00003	10.4	0.34	10.4	0.20
2497-1B	0.702505	0.00003	0.70245	0.00004	10.4	0.34	10.1	0.20

[a]*Sims et al.* [2002, 2003]. Precision estimates (2σ) reflect long-term analyses of NBS 987 Sr standard (±0.00003) and JNdiNd standard (±0.34). Reproducibilities for published data are ±20–30 ppm (±0.00003–0.00006) and ±0.20 ε_{Nd} units [*Sims et al.*, 2002, 2003].
[b]Published ε_{Nd} units corrected for long-term error (see Waters et al., submitted manuscript, 2010).

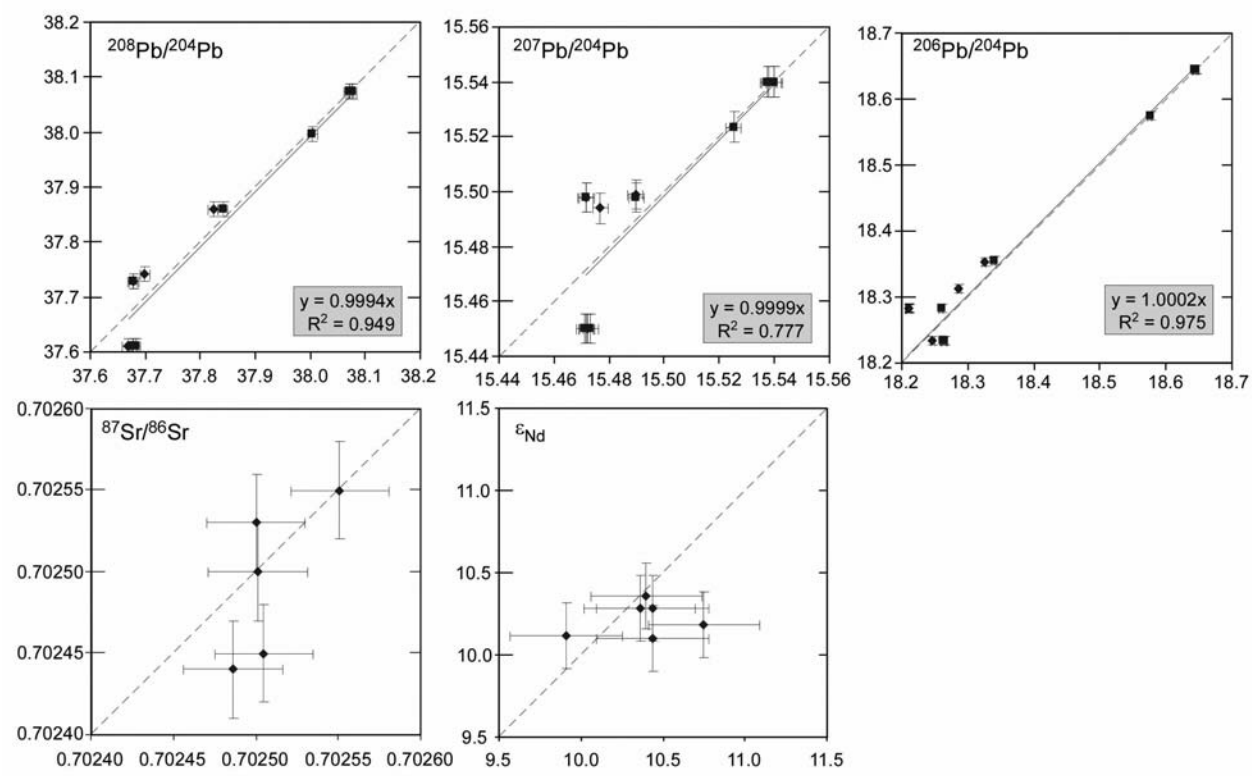

Figure B1. Plots showing analytical reproducibility for 8°N–10°N EPR basaltic glass Pb, Sr, and Nd isotopic ratios from the University of Florida (*x* axis) versus published ratios from *Sims et al.* [2002, 2003] (*y* axis). All data shown in Tables B1a and B1b. Error bars represent 2σ long-term analytical uncertainties. Shaded diamonds and squares mark separate machine runs in February 2008 and April 2008, respectively. Dashed line shows the ideal 1:1 replication curve, whereas the solid line in the Pb isotope plots is a linear (b = 0) regression line through the data.

isotopic ratios were measured following the Tl mass bias normalization technique of *Kamenov et al.* [2004] and normalized relative to values of NBS 981 reported by *Todt et al.* [1996] ($^{206}Pb/^{204}Pb$ = 16.9356; $^{207}Pb/^{204}Pb$ = 15.4891; $^{208}Pb/^{204}Pb$ = 36.7006). Long-term values and 2σ reproducibility of NBS 981 (n = 38; June 2007 to April 2008) are $^{206}Pb/^{204}Pb$ = 16.9361 ± 0.0034 (±205 ppm), $^{207}Pb/^{204}Pb$ = 15.4883 ± 0.0028 (±184 ppm), and $^{208}Pb/^{204}Pb$ = 36.6889 ± 0.0086 (±234 ppm). Lead concentrations in procedural blanks measured along with unknowns ranged from ~10 to 50 pg. Nd isotopes were measured in static "time resolved analysis" (TRA) mode following the analytical method developed by *Kamenov et al.* [2006, 2008]. The measured ^{144}Nd, ^{148}Nd, and ^{150}Nd beams were corrected for isobaric interference from Sm using $^{147}Sm/^{144}Sm$ = 4.88, $^{147}Sm/^{148}Sm$ = 1.33, and $^{147}Sm/^{150}Sm$ = 2.03. All measured ratios were normalized to $^{146}Nd/^{144}Nd$ = 0.7219 using an exponential law for mass bias fractionation. Baseline was measured by ESA (electrostatic analyzer) deflection of the beam. Long-term analysis of the JNdi-1 Nd standard yielded an average $^{143}Nd/^{144}Nd$ value and 2σ reproducibility of 0.512099 ± 0.000018. Unknowns were normalized to an $^{143}Nd/^{144}Nd$ value of 0.512115 ± 0.000007 for JNdi-1, which is reported by *Tanaka et al.* [2000] relative to a La Jolla $^{143}Nd/^{144}Nd$ value of 0.511858 [*Lugmair and Carlson*, 1978].

[58] Replicate Sr isotopic ratios were obtained both via MC-ICPMS and VG Sector 54 Thermal Ionization Mass Spectrometer (TIMS) at the University of Florida. A direct comparison of the data is shown in Appendix B. MC-ICPMS analyses were also run in static TRA mode following protocols described by *Kamenov et al.* [2006, 2008]. For both analytical methods, mass bias was corrected to $^{88}Sr/^{86}Sr$ = 0.1194 using the exponential fractionation law. Repeat analyses of NBS 987 Sr standard yielded average values of 0.710255 ± 0.000026 and 0.710247 ± 0.000013 for MC-ICPMS and TIMS, respectively. Reported long-term average $^{87}Sr/^{86}Sr$ values and 2σ reproducibility of NBS 987

Table C1. Comparison of TIMS Versus MC-ICPMS $^{87}Sr/^{86}Sr$ Data[a]

	TIMS				MC-ICPMS[b]	
	In Run					
Sample	$^{87}Sr/^{88}Sr$	% Standard Error	2σ	Long-Term 2σ	$^{87}Sr/^{88}Sr$	Long-Term 2σ
2384-3	0.7025967	0.0010	0.000014	0.000020	0.702543	0.00003
2392-9	0.7024799	0.0009	0.000013	0.000020	0.702492	0.00003
2497-1b	-	-	-	-	-	0.00003
2752-6	0.7024935	0.0008	0.000011	0.000020	0.702478	0.00003
2759-14	0.7024770	0.0008	0.000011	0.000020	0.702493	0.00003
4202-2a	0.7024761	0.0008	0.000011	0.000020	0.702457	0.00003
4202-6	0.7024751	0.0009	0.000013	0.000020	0.702493	0.00003
4203-2	0.7024633	0.0008	0.000011	0.000020	0.702463	0.00003
4204-1	0.7024710	0.0009	0.000013	0.000020	0.702482	0.00003
4204-2	0.7024788	0.0008	0.000011	0.000020	0.702498	0.00003
4204-3	0.7024939	0.0008	0.000011	0.000020	0.702510	0.00003
4204-4a	0.7024882	0.0008	0.000011	0.000020	0.702487	0.00003
4204-4b	0.7024751	0.0008	0.000011	0.000020	0.702485	0.00003
4204-8	0.7024812	0.0009	0.000013	0.000020	0.702514	0.00003
4204-9	0.7024817	0.0009	0.000013	0.000020	0.702481	0.00003
4205-6	0.7024742	0.0007	0.000010	0.000020	0.702497	0.00003
4206-2	0.7024681	0.0008	0.000011	0.000020	0.702462	0.00003
D48A	0.7024755	0.0008	0.000011	0.000020	0.702475	0.00003
2497-1b	0.7024825	0.0008	0.000011	0.000020	0.702497	0.00003
D48B	0.7024801	0.0008	0.000011	0.000020	0.702478	0.00003

	TIMS		MC-ICPMS[b]	
	$^{87}Sr/^{88}Sr$	2σ	$^{87}Sr/^{88}Sr$	2σ
2005–2006 average (n = 13)	0.7024760	0.000013	0.7024824	0.000016

[a]In-run NBS 987_{TIMS} = 0.7102475±0.000013. In-run NBS $987_{MC\text{-}ICPMS}$ = 0.7102552 ± 0.000026.
[b]MC-ICPMS $^{87}Sr/^{86}Sr$ ratios normalized to the in-run NBS 987_{TIMS} to facilitate data comparison.

are indistinguishable for MC-ICPMS (0.710246 ± 0.000030, or 42 ppb) and TIMS (0.71024 ± 0.000020, or 28 ppb [*Hodell et al.*, 2004]).

Appendix B: Comparison With Published Isotopic Data

[59] To facilitate comparison of our new isotopic data from the 2005–2006 EPR eruption with published data from older (>8000 years to 1991) 8°–10° EPR lava flows [*Sims et al.*, 2002, 2003], replicate analyses of 8 basaltic glass samples were obtained at the University of Florida and include (1) both on- and off-axis N-MORB lavas from 9°N to 10°N along the EPR [*Sims et al.*, 2002, 2003], (2) incompatible element-depleted and enriched lavas (D-MORB and E-MORB, respectively) from the Siqueiros Transform [*Sims et al.*, 2002] at 8°20′N, and (3) off-axis E-MORB lavas from ~9°30′N (Waters et al., submitted manuscript, 2010) (Tables B1a and B1b). In general, these data show excellent correlation for all measured isotopic ratios with the majority of samples plotting along the ideal 1:1 reproducibility curve. Linear regression analysis between new and published $^{206}Pb/^{204}Pb$, $^{207}Pb/^{204}Pb$, and $^{208}Pb/^{204}Pb$ ratios yield R^2 values of 0.975, 0.777, and 0.949, respectively (Figure B1). Similarly, the majority of $^{87}Sr/^{86}Sr$ and ε_{Nd} (corrected for in-lab drift from published values (K. W. W. Sims, personal communication, 2008)) replicate analyses (Sr − 3 of 5; ε_{Nd} 4 of 5) are statistically identical. Based on these comparative analyses, new isotopic data from the 2005–2006 eruption along the 9°50′N segment of the EPR can be directly compared to existing data from older EPR eruptions. Moreover, our results confirm the anomalously enriched isotopic ratios for Siqueiros Transform D-MORB and E-MORB basalts previously discussed by *Sims et al.* [2002].

Appendix C: $^{87}Sr/^{86}Sr$—MC-ICPMS Versus TIMS

[60] In the past, Thermal Ionization Mass Spectrometry (TIMS) has been the analytical tool of choice for high-precision $^{87}Sr/^{86}Sr$ measurements, particularly for rocks with relatively low Sr concentrations (i.e., peridotites, MORB). Efficient filament ionization and accurate monitoring and correction of in-run mass fractionations have sustained long-term 2σ reproducibilities of $\leq \pm 50$ ppm

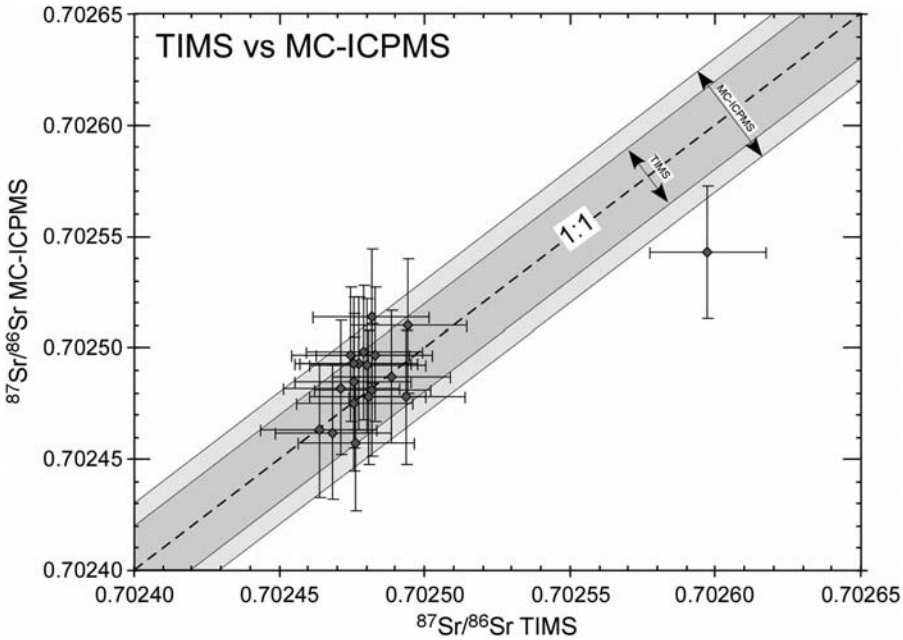

Figure C1. Graph showing comparison between TIMS and MC-ICPMS $^{87}Sr/^{86}Sr$ data for <100 years old and 2005–2006 basalt glasses from ~9°50N EPR. The anomalously enriched sample is from a young (<100 years) glassy pillow lava from the Siqueiros Transform (2384-3). Error bars reflect long-term reproducibility of NBS 987 and are ±0.00003 and 0.00003 for TIMS and MC-ICPMS, respectively. Dashed line shows the ideal 1:1 replication curve, with error limits for both methods outlined by shaded fields.

for Sr isotopic analysis [*Walczyk*, 2004]. However, to achieve such highly precise $^{87}Sr/^{86}Sr$ determinations on a Micromass S-54 TIMS, a single sample takes on the order of 2–3 h due to the long acquisition time (~30 s) required to generate a statistically necessary number of ratio measurements (n = 100–120) for such high-precision analysis [*Ludwig*, 1997]. The advent of inductively coupled plasma mass spectrometers introduced an entirely new ionization mechanism of sample media, aspiration of a dilute acid with into a charged plasma ion source. However, rapid shifts in signal intensity due to nonsteady gas flow and variable plasma stability limited its application for high-precision isotopic ratios of the heavier elements. The use of ICP-MS equipped with multiple collectors (MC-ICPMS) solves this problem as simultaneous detection of multiple ion beams, each with an individual mass, cancels out error caused by flickers in signal intensity [*Walder et al.*, 1993]. Typical or "traditional" isotopic analysis on a Nu-Plasma MC-ICPMS requires an integration time of ~10 s, or 10–15 min per analysis to generate data with precision of ± 60 ppm [*Kamenov et al.*, 2008]. Though the time for this type of measurement is an order of magnitude less than traditional TIMS, the more than twofold loss in analytical precision excludes its use in geological systems with isotopic heterogeneity of <60 ppm or for samples with low Sr concentrations (i.e., few nanograms).

[61] In order to increase the precision limits to those normally obtained by TIMS, MORB glasses from the 2005–2006 EPR eruption at ~9°50′N were analyzed for $^{87}Sr/^{86}Sr$ using the TRA method described in detail by *Kamenov et al.* [2008]. This is achieved by acquiring data in 0.2 s integrations, yielding 120 integrations per minute and acquiring optimal precision in ~100 s (i.e., where additional integration time does not significantly improve the error). Such short analyses generate greater precision than "traditional" methods due to more stable ion beam ratios affected by less significant changes in the mass bias. Moreover, rapid "on-peak" zero measurement followed immediately by sample signal reduces the error caused by fluctuations in the isobaric interference of Kr (a contaminant in the Ar gas) on the $^{87}Sr/^{86}Sr$ ratio. This is reflected in a ~30% improvement in analytical precision for TRA-obtained $^{87}Sr/^{86}Sr$ ratios (42 ppm) compared to traditional MC-ICPMS (60 ppm) and approaches our long-term TIMS precision (28 ppm).

[62] To assess the analytical precision between MC-ICPMS and TIMS for a suite of real geologi-

cal samples, replicate TIMS-obtained $^{87}Sr/^{86}Sr$ analyses are given in Table C1 and plotted against the MC-ICPMS data in Figure C1. To facilitate the data comparison, MC-ICPMS-obtained ratios have been normalized to the in-run TIMS NBS 987 Sr standard. Results show that virtually all (18 of 19) corrected MC-ICPMS $^{87}Sr/^{86}Sr$ ratios fall within the TIMS-defined error limits of the 1:1 unity line and are thus statistically identical to the values obtained by TIMS. Only one MC-ICPMS $^{87}Sr/^{86}Sr$ ratio from the Siqueiros Transform (2384-3) falls outside of the error limits of a replicate TIMS analysis, though both analyses are within the $^{87}Sr/^{86}Sr$ error limits reported by *Sims et al.* [2002] for this sample (0.70255 ± 0.00006). Based on these data, neither analytical methodology can resolve any isotopic heterogeneity within the $^{87}Sr/^{86}Sr$ data field defined by the 2005–2006 EPR eruption. Moreover, the average $^{87}Sr/^{86}Sr$ ratios of all 2005–2006 lavas (MC-ICPMS: 0.7024905 ± 0.000016 and TIMS: 0.7024760 ± 0.000013, 2σ) cannot be resolved within the error limits of both methodologies. In light of these results, time resolved MC-ICPMS analysis provides a rapid technique of obtaining high-quality $^{87}Sr/^{86}Sr$ ratios on MORB glasses without a noticeable reduction in analytical precision compared to traditional TIMS.

Acknowledgments

[63] We thank the officers and crews of the R/V *Knorr*, R/V *New Horizon*, R/V *Atlantis*, and *Alvin* shipboard operations groups, who all contributed to the success of 2005–2006 East Pacific Rise eruptions expeditionary campaigns as well as the other chief scientists for the cruises, J. Cowen, K. Von Damm, T. Shank, S. White, and E. Klein. Two constructive reviews by Lawrence Coogan and Emily Klein improved the final version of this manuscript, as did numerous discussions with V. Dorsey Wanless and Bailey Trump. This work has been supported by NSF grants OCE-0525863 and OCE-0732366 (D. J. Fornari and S. A. Soule), OCE-0636469 (K. H. Rubin), and OCE-0138088 (M. R. Perfit), as well as postdoctoral fellowship funds from the University of Florida. W.I.R. publishes with permission of the Director, U. S. Geological Survey.

References

Alexander, R. T., and K. C. Macdonald (1996), Small off-axis volcanoes on the East Pacific Rise, *Earth Planet. Sci. Lett.*, *139*(3–4), 387–394, doi:10.1016/0012-821X(96)00028-3.

Asimow, P. D., and M. S. Ghiorso (1998), Algorithmic modifications extending MELTS to calculate subsolidus phase relations, *Am. Mineral.*, *83*, 1127–1131.

Batiza, R., and Y. Niu (1992), Petrology and magma chamber processes at the East Pacific Rise ~9°30′N, *J. Geophys. Res.*, *97*(B5), 6779–6797, doi:10.1029/92JB00172.

Bergmanis, E., J. Sinton, and K. H. Rubin (2007), Recent eruptive history and magma reservoir dynamics on the southern East Pacific Rise at 17°30′S, *Geochem. Geophys. Geosyst.*, *8*, Q12O06, doi:10.1029/2007GC001742.

Boudier, F., A. Nicolas, and B. Ildefonse (1996), Magma chambers in the Oman ophiolite: Fed from the top and the bottom, *Earth Planet. Sci. Lett.*, *144*(1–2), 239–250, doi:10.1016/0012-821X(96)00167-7.

Bougault, H., and R. Hekinian (1974), Rift valley in Atlantic Ocean near 36°50′N: Petrology and geochemistry of basaltic rocks, *Earth Planet. Sci. Lett.*, *24*(2), 249–261, doi:10.1016/0012-821X(74)90103-4.

Bowles, J., J. S. Gee, D. V. Kent, M. R. Perfit, A. Soule, and D. J. Fornari (2006), Paleointensity results from 9°–10°N on the East Pacific Rise: Implications for timing and extent of eruptive activity, *Geochem. Geophys. Geosyst.*, *8*, Q06006, doi:10.1029/2005GC001141.

Buck, W. R., L. L. Lavier, and A. N. B. Poliakov (2005), Modes of faulting at mid-ocean ridges, *Nature*, *434*, 719–723, doi:10.1038/nature03358.

Canales, J. P., R. S. Detrick, D. R. Toomey, and W. S. D. Wilcock (2003), Segment-scale variations in the crustal structure of 150–300 kyr old fast spreading oceanic crust (East Pacific Rise, 8°15′N–10°5′N) from wide-angle seismic refraction profiles, *Geophys. J. Int.*, *152*(3), 766–794, doi:10.1046/j.1365-246X.2003.01885.x.

Canales, J. P., S. M. Carbotte, J. C. Mutter, M. R. Nedimović, H. Carton, M. Xu, K. Newman, O. Aghaei, M. Marjanović, and L. Stowe (2008), Discovery of off-axis melt lenses at the RIDGE-2000 East Pacific Rise Integrated Studies Site, *Eos Trans. AGU*, *89*(53), Fall Meet. Suppl., Abstract B21A-0319.

Canales, J. P., M. R. Nedimovic, M. K. Graham, S. M. Carbotte, and R. S. Detrick (2009), Seismic reflection images of a near-axis melt sill within the lower crust at the Juan de Fuca ridge, *Nature*, *460*, 89–94, doi:10.1038/nature08095.

Carbotte, S., and K. Macdonald (1992), East Pacific Rise 8°–10°30′N: Evolution of ridge segments and discontinuities from SeaMARC II and three-dimensional magnetic studies, *J. Geophys. Res.*, *97*, 6959–6982, doi:10.1029/91JB03065.

Carbotte, S. M., J. C. Mutter, and L. Xu (1997), Contribution of volcanism and tectonism to axial and flank morphology of the southern East Pacific Rise, 17°10′–17°40′S, from a study of layer 2A geometry, *J. Geophys. Res.*, *102*, 10,165–10,184, doi:10.1029/96JB03910.

Carbotte, S., C. Mutter, J. Mutter, and G. Ponce-Correa (1998), Influence of magma supply and spreading rate on crustal magma bodies and emplacement of the extrusive layer: Insights from the east Pacific rise at lat16°N, *Geology*, *26*(5), 455–458, doi:10.1130/0091-7613(1998)026<0455:IOMSAS>2.3.CO;2.

Carbotte, S. M., A. Solomon, and G. Ponce-Correa (2000), Evaluation of morphological indicators of magma supply and segmentation from a seismic reflection study of the East Pacific Rise 15°30′–17°N, *J. Geophys. Res.*, *105*(B2), 2737–2759, doi:10.1029/1999JB900245.

Carbotte, S. M., J. C. Mutter, J. P. Canales, M. R. Nedimovic, H. Carton, M. Xu, K. Newman, M. Marjanovic, O. Aghaei, and L. Stowe (2008), New observations of the magmatic segmentation of the East Pacific Rise from Siquieros to Clipperton from a multi-streamer seismic reflection imaging

study, *Eos Trans. Trans.*, *89*(53), Fall Meet. Suppl., Abstract B21A-0320.

Carbotte, S. M., M. R. Perfit, J. B. Gill, D. Kelley, J. P. Canales, M. R. Nedimovic, and H. Carton (2009), Near-axis melt anomalies and segmentation of axial melt: A common framework for the EPR and Endeavour ISS?, *Eos Trans. AGU*, *90* (52), Fall Meet. Suppl., Abstract OS11B-01.

Caress, D. W., M. S. Burnett, and J. A. Orcutt (1992), Tomographic image of the axial low-velocity zone at 12 50′ N on the East Pacific Rise, *J. Geophys. Res.*, *97*, 9243–9263, doi:10.1029/92JB00287.

Castillo, P. R., J. W. Hawkins, P. F. Lonsdale, D. R. Hilton, A. M. Shaw, and M. D. Glascock (2002), Petrology of Alarcon Rise lavas, Gulf of California: Nascent intracontinental ocean crust, *J. Geophys. Res.*, *107*(B10), 2222, doi:10.1029/2001JB000666.

Chadwick, W. W., R. W. Embley, H. B. Milburn, C. Meinig, and M. Stapp (1999), Evidence for deformation associated with the 1998 eruption of Axial Volcano, Juan de Fuca Ridge, from acoustic extensometer measurements, *Geophys. Res. Lett.*, *26*(23), 3441–3444, doi:10.1029/1999GL900498.

Christeson, G. L., G. M. Purdy, and G. J. Fryer (1994), Seismic constraints on shallow crustal emplacement processes at the fast-spreading East Pacific Rise, *J. Geophys. Res.*, *99*, 17,957–17,973, doi:10.1029/94JB01252.

Christeson, G. L., G. M. Kent, G. M. Purdy, and R. S. Detrick (1996), Extrusive thickness variability at the East Pacific Rise, 9°–10°N: Constraints from seismic techniques, *J. Geophys. Res.*, *101*, 2859–2873, doi:10.1029/95JB03212.

Conrad, C. P., and C. Lithgow-Bertelloni (2002), How mantle slabs drive plate tectonics, *Science*, *298*, 207–210, doi:10.1126/science.1074161.

Cowen, J. P., et al. (2007), Volcanic eruptions at the East Pacific Rise near 9°50′N, *Eos Trans. AGU*, *88*, 81–83, doi:10.1029/2007EO070001.

Crawford, W. C., and S. C. Webb (2002), Variations in the distribution of magma in the lower crust and at the Moho beneath the East Pacific Rise at 9°–10°N, *Earth Planet. Sci. Lett.*, *203*(1), 117–130, doi:10.1016/S0012-821X(02)00831-2.

Crawford, W. C., S. C. Webb, and J. A. Hildebrand (1999), Constraints on melt in the lower crust and Moho a the East Pacific Rise, 9°48′N, using seafloor compliance measurements, *J. Geophys. Res.*, *104*, 2923–2939, doi:10.1029/1998JB900087.

Danyushevsky, L. (2001), The effect of small amounts of H_2O on crystallization of mid-ocean ridge and backarc basin magmas, *J. Volcanol. Geotherm. Res.*, *110*, 265–280, doi:10.1016/S0377-0273(01)00213-X.

Detrick, R. S., P. Buhl, E. E. Vera, J. C. Mutter, J. A. Orcutt, J. A. Madsen, and T. M. Brocher (1987), Multi-channel seismic imaging of a crustal magma chamber along the East Pacific Rise, *Nature*, *326*(6108), 35–41, doi:10.1038/326035a0.

Dunn, T., and C. Sen (1994), Mineral/matrix partition-coefficients for ortho-pyroxene, plagioclase, and olivine in basaltic to andesitic systems—A combined analytical and experimental study, *Geochim. Cosmochim. Acta*, *58*(2), 717–733, doi:10.1016/0016-7037(94)90501-0.

Dziak, R. P., D. R. Bohnenstiehl, H. Matsumoto, M. J. Fowler, J. H. Haxel, M. Tolstoy, and F. Waldhauser (2009), January 2006 seafloor-spreading event at 9° 50′ N, East Pacific Rise: Ridge dike intrusion and transform fault interactions from regional hydroacoustic data, *Geochem. Geophys. Geosyst.*, *10*, Q06T06, doi:10.1029/2009GC002388.

Eason, D., and J. M. Sinton (2006), Origin of high-Al N-MORB by fractional crystallization in the upper mantle beneath the Galápagos Spreading Center, *Earth Planet. Sci. Lett.*, *252*, 423–436, doi:10.1016/j.epsl.2006.09.048.

Elthon, D. (1993), The crystallization of mid-ocean ridge basalts at moderate and high pressures, *Eur. J. Mineral.*, *5*, 1025–1037.

Embley, R. W., W. W. Chadwick, M. R. Perfit, M. C. Smith, and J. R. Delaney (2000), Recent eruptions on the CoAxial segment of the Juan de Fuca Ridge: Implications for mid-ocean ridge accretion processes, *J. Geophys. Res.*, *105* (B7), 16,501–16,525, doi:10.1029/2000JB900030.

Escartín, J., A. Soule, D. J. Fornari, M. A. Tivey, H. Schouten, and M. R. Perfit (2007), Interplay between faults and lava flows in construction of the upper oceanic crust: The East Pacific Rise crest 9°25′–9°58′N, *Geochem. Geophys. Geosyst.*, *8*, Q06005, doi:10.1029/2006GC001399.

Faure, F., and P. Schianoa (2004), Crystal morphologies in pillow basalts: Implications for mid-ocean ridge processes, *Earth Planet. Sci. Lett.*, *220*(3–4), 331–344, doi:10.1016/S0012-821X(04)00057-3.

Fornari, D. J. (2003), A new deep-sea towed digital camera and multi-rock coring system, *Eos Trans. AGU*, *84*, 69–76, doi:10.1029/2003EO080001.

Fornari, D. J., M. R. Perfit, J. F. Allan, R. Batiza, R. Haymon, A. Barone, W. B. F. Ryan, T. Smith, T. Simkin, and M. A. Luckman (1988), Geochemical and structural studies of the Lamont Seamount: Seamounts as indicators of mantle processes, *Earth Planet. Sci. Lett.*, *89*(1), 63–83, doi:10.1016/0012-821X(88)90033-7.

Fornari, D. J., R. M. Haymon, M. R. Perfit, T. K. P. Gregg, and M. H. Edwards (1998), Axial summit trough of the East Pacific Rise 9°–10°N: Geological characteristics and evolution of the axial zone on fast spreading mid-ocean ridges, *J. Geophys. Res.*, *103*(B5), 9827–9855, doi:10.1029/98JB00028.

Fornari, D., M. Tivey, H. Schouten, M. Perfit, D. Yoerger, K. L. Von Damm, T. Shank, and A. Soule (2004), Submarine lava flow emplacement at the East Pacific Rise 9°50′N: Implications for uppermost ocean crust stratigraphy and hydrothermal fluid circulation, in *Mid-Ocean Ridges: Hydrothermal Interactions Between the Lithosphere and Oceans*, *Geophys. Monogr. Ser.*, vol. 148, edited by C. R. German, J. Lin, and L. M. Parson, pp. 187–217, AGU, Washington, D. C.

Francheteau, J., R. Armijo, J. L. Cheminee, R. Henikian, P. Lonsdale, and N. Blum (1990), 1 Ma East Pacific Rise oceanic crust and uppermost mantle exposed by rifting in Hess Deep (equatorial Pacific Ocean), *Earth Planet. Sci. Lett.*, *101*, 281–285, doi:10.1016/0012-821X(90)90160-Y.

Fundis, A. T., S. A. Soule, D. J. Fornari, and M. R. Perfit (2008), The 2005–2006 eruption at the East Pacific Rise 9°50′N: Detailed flow morphology mapping and insight into emplacement processes, *Eos Trans. AGU*, *89*(53), Fall Meet. Suppl., Abstract B21A-0328.

Gao, Y., J. Hoefs, E. Hellebrand, A. von der Handt, and J. E. Snow (2007), Trace element zoning in pyroxenes from ODP Hole 735B gabbros: Diffusive exchange or synkinematic crystal fractionation, *Contrib. Mineral. Petrol.*, *153*, 429–442, doi:10.1007/s00410-006-0158-4.

Garcia, M. O., R. A. Ho, J. M. Rhodes, and E. W. Wolfe (1989), Petrologic constraints on rift-zone processes, *Bull. Volcanol.*, *52*(2), 81–96, doi:10.1007/BF00301548.

Garcia, M. O., A. Pietruszka, J. M. Rhodes, and K. Swanson (2000), Magmatic processes during prolonged Pu'u O'o

eruption of Kilauea volcano, Hawaii, *J. Petrol.*, *41*(7), 967–990, doi:10.1093/petrology/41.7.967.

Garmany, J. (1989), Accumulations of melt at the base of young oceanic crust, *Nature*, *340*(6235), 628–632, doi:10.1038/340628a0.

Geshi, N., S. Umino, H. Kumagai, J. M. Sinton, S. M. White, K. Kisimoto, and T. W. Hilde (2007), Discrete plumbing systems and heterogeneous magma sources of a 24 km^3 off-axis lava field on the western flank of East Pacific Rise, 14° S, *Earth Planet. Sci. Lett.*, *258*(1–2), 61–72, doi:10.1016/j.epsl.2007.03.019.

Ghiorso, M. S., and R. O. Sack (1995), Chemical mass transfer in magmatic processes IV: A revised and internally consistent thermodynamic model for the interpolation and extrapolation of liquid-solid equilibria in magmatic systems at elevated temperatures and pressures, *Contrib. Mineral. Petrol.*, *119*, 197–212, doi:10.1007/BF00307281.

Goldstein, S. J., M. T. Murrell, and R. W. Williams (1993), ^{231}Pa and ^{230}Th chronology of mid-ocean ridge basalts, *Earth Planet. Sci. Lett.*, *115*, 151–160, doi:10.1016/0012-821X(93)90219-Y.

Goldstein, S. J., M. R. Perfit, R. Batiza, D. J. Fornari, and M. T. Murrell (1994), Off-axis volcanism at the East Pacific Rise detected by uranium-series dating of basalts, *Nature*, *367* (6459), 157–159, doi:10.1038/367157a0.

Goss, A. R., S. M. Kay, C. Mpodozis, and B. Singer (2009), The Incapillo Caldera (~28°S): A stranded magma chamber over a dying Andean arc, *J. Volcanol. Geotherm. Res.*, *184*, 389–404, doi:10.1016/j.jvolgeores.2009.05.005.

Gregg, P. M., M. D. Behn, J. Lin, and T. L. Grove (2009), Melt generation, crystallization, and extraction beneath segmented oceanic transform faults, *J. Geophys. Res.*, *114*, B11102, doi:10.1029/2008JB006100.

Gregg, T. K. P., D. J. Fornari, M. R. Perfit, R. M. Haymon, and J. H. Fink (1996), Rapid emplacement of a mid-ocean ridge lava flow on the East Pacific Rise at 9°46′–51′N, *Earth Planet. Sci. Lett.*, *144*, E1–E7, doi:10.1016/S0012-821X(96)00179-3.

Grove, T. L., R. J. Kinzler, and W. B. Bryan (1992), Fractionation of mid-ocean ridge basalts, in *Mantle Flow and Melt Generation at Mid-Ocean Ridges*, *Geophys. Monogr. Ser.*, vol. 71, edited by J. Phipps Morgan, D. Blackman, and J. Sinton, pp. 281–310, AGU, Washington, D. C.

Hall, L. S., and J. M. Sinton (1996), Geochemical diversity of the large lava field on the flank of the East Pacific Rise at 8° 17'S, *Earth Planet. Sci. Lett.*, *142*(1–2), 241–251, doi:10.1016/0012-821X(96)00089-1.

Halliday, A. N., D. C. Lee, S. Tommasini, G. R. Davies, C. R. Paslick, J. G. Fitton, and D. E. James (1995), Incompatible trace-elements in OIB and MORB and source enrichment in the sub-oceanic mantle, *Earth Planet. Sci. Lett.*, *133*(3–4), 379–395, doi:10.1016/0012-821X(95)00097-V.

Harding, A. J., G. M. Kent, M. M. Kappus, J. A. Orcutt, E. E. Vera, J. C. Buhl, J. C. Mutter, R. S. Detrick, and T. Brocher (1989), The structure of young oceanic crust at 13° N on the East Pacific Rise from expanding spread profiles, *J. Geophys. Res.*, *94*, 12,163–12,196, doi:10.1029/JB094iB09p12163.

Harding, A. J., G. M. Kent, and J. A. Orcutt (1993), A multichannel seismic investigation of upper crustal structure at 9° N on the East Pacific Rise, *J. Geophys. Res.*, *98*, 13,925–13,944, doi:10.1029/93JB00886.

Haymon, R. M., D. J. Fornari, M. H. Edwards, S. M. Carbotte, D. Wright, and K. C. MacDonald (1991), Hydrothermal vent distribution along the East Pacific Rise crest (9°09′–54′N) and its relationship to magmatic and tectonic processes on fast-spreading mid-ocean ridges, *Earth Planet. Sci. Lett.*, *104*(2–4), 513–534, doi:10.1016/0012-821X(91)90226-8.

Haymon, R. M., et al. (1993), Volcanic eruption of the mid-ocean ridge along the East Pacific Rise crest at 9°45–52′N: Direct submersible observations of seafloor phenomena associated with an eruption event in April, 1991, *Earth Planet. Sci. Lett.*, *119*(1–2), 85–101, doi:10.1016/0012-821X(93)90008-W.

Hekinian, R., G. Thompson, and D. Bideau (1989), Axial and off-axial heterogeneity of basaltic rocks from the East Pacific Rise at 12°35′N–12°51′N and 11°26′–11°30′N, *J. Geophys. Res.*, *94*, 17,437–17,463, doi:10.1029/JB094iB12p17437.

Hekinian, R., D. Bideau, J. Francheteau, J. L. Cheminee, R. Armijo, P. Lonsdale, and N. Blum (1993), Petrology of the East Pacific Rise Crust and upper mantle exposed in Hess Deep (eastern equatorial Pacific), *J. Geophys. Res.*, *98*(B5), 8069–8094, doi:10.1029/92JB02072.

Herzberg, C. (2004), Partial crystallization of Mid-Ocean Ridge basalts in the crust and mantle, *J. Petrol.*, *45*(12), 2389–2405, doi:10.1093/petrology/egh040.

Hodell, D. A., R. L. Quinn, M. Brenner, and G. D. Kamenov (2004), Spatial variation of strontium isotopes ($^{87}Sr/^{86}Sr$) in the Maya region: A tool for tracking ancient human migration, *J. Archaeol. Sci.*, *31*, 585–601, doi:10.1016/j.jas.2003.10.009.

Hooft, E. E. E., H. Schouten, and R. S. Detrick (1996), Constraining crustal emplacement processes from the variation in seismic layer 2A thickness at the East Pacific Rise, *Earth Planet. Sci. Lett.*, *142*, 289–309, doi:10.1016/0012-821X(96)00101-X.

Kamenov, G. D., P. Mueller, and M. R. Perfit (2004), Optimization of mixed Pb-Tl solutions for high precision isotopic analyses by MC-ICP-MS, *J. Anal. At. Spectrom.*, *19*, 1262–1267, doi:10.1039/b403222e.

Kamenov, G. D., P. A. Mueller, A. Gilli, S. Coynet, and S. H. H. Nielsen (2006), A simple method for rapid, high-precision isotope analysis of small samples by MC-ICPMS, *Eos Trans. AGU*, *87*(52), Fall Meet. Suppl., Abstract V21A-0542.

Kamenov, G. D., M. R. Perfit, P. A. Mueller, and I. R. Jonasson (2008), Controls on magmatism in an island arc environment: Study of lavas and sub-arc xenoliths from the Tabar-Lihir-Tanga-Feni island chain, Papua New Guinea, *Contrib. Mineral. Petrol.*, *155*, 635–656, doi:10.1007/s00410-007-0262-0.

Karson, J. A., E. M. Klein, S. D. Hurst, C. Lee, P. Rivizzigno, D. Curewitz, A. R. Morris, and H. D. S. Party (2002), Structure of uppermost fast-spread oceanic crust exposed at the Hess Deep Rift: Implications for subaxial processes at the East Pacific Rise, *Geochem. Geophys. Geosyst.*, *3*(1), 1002, doi:10.1029/2001GC000155.

Kelemen, P. B., K. Koga, and N. Shimizu (1997), Geochemistry of gabbro sills in the crust-mantle transition zone of the Oman Ophiolite: Implications for the origin of the oceanic lower crust, Earth Planet. *Sci. Lett.*, *146*(3–4), 475–488, doi:10.1016/S0012-821X(96)00235-X.

Kent, G. M., A. J. Harding, and J. A. Orcutt (1990), Evidence for a smaller magma chamber beneath the East Pacific Rise at 9°30′N, *Nature*, *344*(6267), 650–653, doi:10.1038/344650a0.

Kent, G. M., A. J. Harding, and J. A. Orcutt (1993a), Distribution of magma beneath the East Pacific Rise near the 9°03′N overlapping spreading center from forward modeling of common depth point data, *J. Geophys. Res.*, *98*(B8), 13,971–13,995.

Kent, G. M., A. J. Harding, and J. A. Orcutt (1993b), Distribution of magma beneath the East Pacific Rise between the Clipperton Transform and the 9°17′N Deval from forward

modeling of common depth point data, *J. Geophys. Res.*, *98* (B8), 13,945–13,970.

Key, K., and S. Constable (2002), Broadband marine MT exploration of the East Pacific Rise at 9° 50′ N, *Geophys. Res. Lett.*, *29*(22), 2054, doi:10.1029/2002GL016035.

Kinzler, R. J., and T. L. Grove (1992), Primary magmas of mid-ocean ridge basalts: 2. Applications, *J. Geophys. Res.*, *97*(B5), 6907–6926, doi:10.1029/91JB02841.

Korenaga, J., and P. B. Kelemen (1997), Origin of gabbro sills in the Moho transition zone of the Oman ophiolite: Implications for magma transport in the oceanic lower crust, *J. Geophys. Res.*, *102*(B12), 27,729–27,749, doi:10.1029/97JB02604.

Langmuir, C. H., J. F. Bender, and R. Batiza (1986), Petrological and tectonic segmentation of the East Pacific Rise, 5°30′–14°30′N, *Nature*, *322*(6078), 422–429, doi:10.1038/322422a0.

Langmuir, C. H., J. F. Bender, and R. Batiza (1990), A trace element enriched province on the East Pacific Rise north of the Orozco transform fault, *Eos Trans. AGU*, *71*(43), 1703.

Langmuir, C., E. Klein, and T. Plank (1992), Petrological systematics of mid-ocean ridge basalts: Constraints on melt generation beneath ocean ridges, in *Mantle Flow and Melt Generation at Mid-Ocean Ridges*, *Geophys. Monogr. Ser.*, vol. 71, edited by J. Phipps Morgan, D. K. Blackman, and J. M. Sinton, pp. 183–280, AGU, Washington, D. C.

Liu, L., and R. P. Lowell (2009), Models of hydrothermal heat output from a convecting, crystallizing, replenished magma chamber beneath an oceanic spreading center, *J. Geophys. Res.*, *114*, B02102, doi:10.1029/2008JB005846.

Ludwig, K. R. (1997), Optimization of multicollector isotope-ratio measurement of strontium and neodymium, *Chem. Geol.*, *135*, 325–334, doi:10.1016/S0009-2541(96)00120-9.

Lugmair, G. W., and R. W. Carlson (1978), The Sm-Nd history of KREEP, *Proc. Lunar Planet. Sci. Conf.*, *9th*, 689–704.

Macdonald, K. C., R. Haymon, and A. Shor (1989), A 220 km^2 recently erupted lava field on the East Pacific Rise near lat 8°S, *Geology*, *17*, 212–216, doi:10.1130/0091-7613(1989)017<0212:AKRELF>2.3.CO;2.

Macdonald, K. C., et al. (1992), The East Pacific Rise and its flanks 8–18°N: History of segmentation, propagation and spreading direction based on SeaMARC II and SeaBeam studies, *Mar. Geophys. Res.*, *14*(4), 299–344, doi:10.1007/BF01203621.

Macdonald, K. C., P. J. Fox, R. T. Alendander, R. Pockalny, and P. Gente (1996), Volcanic growth faults and the origin of Pacific abyssal hills, *Nature*, *380*, 125–129, doi:10.1038/380125a0.

Machado, N., J. N. Ludden, C. Brooks, and G. Thompson (1982), Fine-scale isotopic heterogeneity in the sub-Atlantic mantle, *Nature*, *295*(5846), 226–228, doi:10.1038/295226a0.

Maclennan, J., D. McKensie, F. Hilton, K. Gronvöld, and N. Shimizu (2003), Geochemical variability in a single flow from northern Iceland, *J. Geophys. Res.*, *108*(B1), 2007, doi:10.1029/2000JB000142.

MacLeod, C. J., F. Boudier, G. Yaouancq, and C. Richter (1996), Gabbro fabrics from Site 894, Hess Deep: Implications for magma chamber processes at the East Pacific Rise, *Proc. Ocean Drill. Program Sci. Results*, *147*, 317–328.

McBirney, A. R. (1995), Mechanisms of differentiation in the Skaergaard intrusion, *J. Geol. Soc.*, *152*, 421–435, doi:10.1144/gsjgs.152.3.0421.

Michael, P. J., and W. C. Cornell (1998), Influence of spreading rate and magma supply on crystallization and assimilation beneath mid-ocean ridges: Evidence from chlorine and major element chemistry of mid-ocean ridge basalts, *J. Geophys. Res.*, *103*(B8), 18,325–18,356, doi:10.1029/98JB00791.

Michael, P. J., M. R. Perfit, A. Palke, D. J. Fornari, and S. A. Soule (2008), Observations of CO_2 exsolution in submarine lava flows: The 2005–6 eruption on the East Pacific Rise, 9° 50″N, *Eos Trans. AGU*, *89*(53), Fall Meet. Suppl., Abstract V21B-2106.

Morton, J. L., H. N. Sleep, W. R. Normark, and D. H. Tomkins (1987), Structure of the southern Juan de Fuca Ridge from seismic reflections records, *J. Geophys. Res.*, *92*, 11,315–11,326, doi:10.1029/JB092iB11p11315.

Nabelek, P. I. (1980), Nickel partitioning between olivine and liquid in natural basalts - Henry's law behavior, *Earth Planet. Sci. Lett.*, *48*(2), 293–302, doi:10.1016/0012-821X(80)90193-4.

Natland, J. H., and H. J. B. Dick (2001), Formation of the lower oceanic crust and the crystallization of gabbroic cumulates at a very slowly spreading ridge, *J. Volcanol. Geotherm. Res.*, *110*(3–4), 191–233, doi:10.1016/S0377-0273(01)00211-6.

Natland, J. H., and H. J. B. Dick (2009), Paired melt lenses at the East Pacific Rise and the pattern of melt flow through the gabbroic layer at a fast-spreading ridge, *Lithos*, *112*, 73–86, doi:10.1016/j.lithos.2009.06.017.

Nicolas, A. (1989), *Structures of Ophiolites and Dynamics of Oceanic Lithosphere*, 367 pp., Kluwer, Dordrecht, Netherlands.

Niu, Y., and R. Batiza (1997), Trace element evidence from seamounts for recycled oceanic crust in the eastern Pacific mantle, *Earth Planet. Sci. Lett.*, *148*, 471–483, doi:10.1016/S0012-821X(97)00048-4.

Nooner, S. L., and W. W. Chadwick (2009), Volcanic inflation measured in the caldera of Axial Seamount: Implications for magma supply and future eruptions, *Geochem. Geophys. Geosyst.*, *10*, Q02002, doi:10.1029/2008GC002315.

Óskarsson, N., G. E. Sigvaldason, and S. Steinthórsson (1982), A dynamic model of rift zone petrogenesis and the regional petrology of Iceland, *J. Petrol.*, *23*(1), 28–74.

Perfit, M. R., and W. W. Chadwick Jr. (1998), Magmatism at mid-ocean ridges: Constraints from volcanological and geochemical investigations, in *Faulting and Magmatism at Mid-Ocean Ridges*, *Geophys. Monogr Ser.*, vol. 106, edited by W. R. Buck, P. T. Delaney, and J. A. Karson, pp. 59–115, AGU, Washington, D. C.

Perfit, M. R., D. J. Fornari, M. C. Smith, J. F. Bender, C. H. Langmuir, and R. M. Haymon (1994a), Small-scale spatial and temporal variations in mid-ocean ridge crest magmatic processes, *Geology*, *22*(4), 375–379, doi:10.1130/0091-7613(1994)022<0375:SSSATV>2.3.CO;2.

Perfit, M. R., M. C. Smith, D. J. Fornari, M. H. Edwards, W. I. Ridley, S. J. Goldstein, J. F. Bender, and R. M. Haymon (1994b), Detailed petrological and geochemical studies of on- and off-axis lavas from the East Pacific Rise; 9°30′–10°N, *Eos Trans. AGU*, *75*(44), Fall Meet. Suppl., 601.

Perfit, M. R., et al. (1996), Recent volcanism in the Siqueiros transform fault: Picritic basalts and implications for MORB magma genesis, *Earth Planet. Sci. Lett.*, *141*, 91–108, doi:10.1016/0012-821X(96)00052-0.

Pin, C. (1997), Sequential separation of rare-earth elements, thorium and uranium by miniaturized extraction chromatography: Application to isotopic analyses of silicate rocks, *Anal. Chim. Acta*, *339*, 79–89, doi:10.1016/S0003-2670(96)00499-0.

Ramondenc, P., L. N. Germanovich, K. L. Von Damm, and R. P. Lowell (2006), The first measurements of hydrothermal heat output at 9°50′N, East Pacific Rise, *Earth Planet. Sci. Lett.*, *245*, 487–497, doi:10.1016/j.epsl.2006.03.023.

Reagan, M. K., J. Gill, E. Malavasi, and M. O. Garcia (1987), Changes in magma composition at Arenal volcano, Costa Rica, 1968–1985: Real-time monitoring of open-system differentiation, *Bull. Volcanol.*, *49*(1), 413–434, doi:410.1007/BF01046634.

Reynolds, J. A., and C. H. Langmuir (2000), Identification and implications of off-axis lava flows around the East Pacific Rise, *Geochem. Geophys. Geosyst.*, *1*(6), 1019, doi:10.1029/1999GC000033.

Reynolds, J. A., C. H. Langmuir, J. F. Bender, K. A. Kastens, and W. B. F. Ryan (1992), Spatial and temporal variability in the geochemistry of basalts from the East Pacific Rise, *Nature*, *359*, 493–499, doi:10.1038/359493a0.

Ridley, W. I., M. R. Perfit, M. C. Smith, and D. J. Fornari (2006), Magmatic processes in developing oceanic crust in a cumulate xenolith collected at the East Pacific Rise, 9°50′N, *Geochem. Geophys. Geosyst.*, *7*, Q12O04, doi:10.1029/2006GC001316.

Ridley, W. I., A. E. Koenig, and M. R. Perfit (2008), Magmatism at the 9°03′N overlapping spreading center, East Pacific Rise: The xenolith story, *Eos Trans. AGU*, *89*(53), Fall Meet. Suppl., Abstract B21A-0331.

Rubin, A. M. (1992), Dike-induced faulting and graben subsidence in volcanic rift zones, *J. Geophys. Res.*, *97*, 1839–1858, doi:10.1029/91JB02170.

Rubin, K., and C. W. Sinton (2007), Inferences on mid-ocean ridge thermal and magmatic structure from MORB compositions, *Earth Planet. Sci. Lett.*, *260*, 257–276, doi:10.1016/j.epsl.2007.05.035.

Rubin, K. H., J. D. Macdougall, and M. R. Perfit (1994), ^{210}Po-^{210}Pb dating of recent volcanic eruptions on the sea floor, *Nature*, *368*(6474), 841–844, doi:10.1038/368841a0.

Rubin, K. H., M. C. Smith, E. C. Bergmanis, M. R. Perfit, J. M. Sinton, and R. Batiza (2001), Geochemical heterogeneity within mid-ocean ridge lava flows: Insights into eruption, emplacement and global variations in magma generation, *Earth Planet. Sci. Lett.*, *188*(3–4), 349–367, doi:10.1016/S0012-821X(01)00339-9.

Rubin, K. H., I. van der Zander, M. C. Smith, and E. C. Bergmanis (2005), Minimum speed limit for ocean ridge magmatism from ^{210}Pb–^{226}Ra–^{230}Th disequilibria, *Nature*, *437*, 534–538, doi:10.1038/nature03993.

Rubin, K. H., M. R. Perfit, D. J. Fornari, S. A. Soule, M. Tolstoy, and F. Waldhauser (2006), Geochronology and composition of the 2005–06 volcanic eruptions of the East Pacific Rise, 9°46′–56′N, *Eos Trans. AGU*, *87*(52), Fall Meet. Suppl., Abstract V23B-0602.

Rubin, K. H., M. Tolstoy, D. J. Fornari, R. P. Dziak, F. Waldhauser, and K. L. Von Damm (2008), Integrating radiometric, geophysical, and thermal signals of volcanic unrest and eruption in 2005–06 at 9°50′N EPR, *Eos Trans. AGU*, *89*(53), Fall Meet. Suppl., Abstract B23F-07.

Rubin, K. H., J. M. Sinton, J. Maclennan, and E. Hellebrand (2009), Magmatic filtering of mantle compositions at mid-ocean-ridge volcanoes, *Nat. Geosci.*, *2*(5), 321–328, doi:10.1038/ngeo504.

Scheirer, D. S., T. M. Shank, and D. J. Fornari (2006), Temperature variations at diffuse and focused flow hydrothermal vent sites along the northern East Pacific Rise, *Geochem. Geophys. Geosyst.*, *7*, Q03002, doi:10.1029/2005GC001094.

Schouten, H., M. A. Tivey, D. J. Fornari, and J. R. Cochran (1999), Central Anomaly Magnetization High: Constraints on the volcanic construction and architecture of seismic layer 2A at a fast-spreading Mid-Ocean Ridge, the EPR at 9°30′–50′N, *Earth Planet. Sci. Lett.*, *169*, 37–50, doi:10.1016/S0012-821X(99)00063-1.

Shank, T. M., D. J. Fornari, K. L. Von Damm, M. D. Lilley, R. M. Haymond, and R. A. Lutz (1998), Temporal and spatial patterns of biological community development at nascent deep-sea hydrothermal vents (9°50′N, East Pacific Rise), *Deep Sea Res., Part II*, *45*, 465–515, doi:10.1016/S0967-0645(97)00089-1.

Shank, T., et al. (2003), Deep submergence synergy: *Alvin* and ABE explore the Galápagos Rift at 86°W, *Eos Trans. AGU*, *84*, 425–440, doi:10.1029/2003EO410001.

Sims, K. W. W., et al. (2002), Chemical and isotopic constraints on the generation and transport of magma beneath the East Pacific Rise, *Geochim. Cosmochim. Acta*, *66*(19), 3481–3504, doi:10.1016/S0016-7037(02)00909-2.

Sims, K. W. W., et al. (2003), Aberrant youth: Chemical and isotopic constraints on the origin of off-axis lavas from the East Pacific Rise, 9°–10°N, *Geochem. Geophys. Geosyst.*, *4*(10), 8621, doi:10.1029/2002GC000443.

Sinton, C. W., and R. S. Detrick (1992), Mid-ocean ridge magma chambers, *J. Geophys. Res.*, *97*, 197–216, doi:10.1029/91JB02508.

Sinton, J. M., S. M. Smaglik, J. J. Mahoney, and K. C. Macdonald (1991), Magmatic processes at superfast spreading mid-ocean ridges: Glass compositional variations along the East Pacific Rise 13°–23°S, *J. Geophys. Res.*, *96*, 6133–6155, doi:10.1029/90JB02454.

Sinton, J., E. Bergmanis, K. Rubin, R. Batiza, T. K. P. Gregg, K. Gronvold, K. C. Macdonald, and S. M. White (2002), Volcanic eruptions on mid-ocean ridges: New evidence from the superfast spreading East Pacific Rise, 17°–19°S, *J. Geophys. Res.*, *107*(B6), 2115, doi:10.1029/2000JB000090.

Smith, M. C., M. R. Perfit, D. J. Fornari, W. I. Ridley, M. E. Edwards, G. Kurras, and K. L. Von Damm (2001), Magmatic processes and segmentation at a fast spreading mid-ocean ridge: Detailed investigation of an axial discontinuity on the East Pacific Rise crest at 9°37′N, *Geochem. Geophys. Geosyst.*, *2*(10), 1040, doi:10.1029/2000GC000134.

Sohn, R. A., J. A. Hildebrand, and S. C. Webb (1999), A microearthquake survey of the high-temperature vent fields on the volcanically active East Pacific Rise, *J. Geophys. Res.*, *104*, 25,367–25,377, doi:10.1029/1999JB900263.

Sohn, R. A., A. H. Barclay, and S. C. Webb (2004), Microearthquakes patterns following the 1998 eruption of Axial Volcano, Juan de Fuca Ridge: Mechanical relaxation and thermal strain, *J. Geophys. Res.*, *109*, B01101, doi:10.1029/2003JB002499.

Soule, S. A., D. J. Fornari, M. R. Perfit, M. A. Tivey, W. I. Ridley, and H. Schouten (2005), Channelized lava flows at the East Pacific Rise crest, 9°–10°N: The importance of off-axis lava transport in developing the architecture of young oceanic crust, *Geochem. Geophys. Geosyst.*, *6*, Q08005, doi:10.1029/2005GC000912.

Soule, S. A., D. J. Fornari, M. R. Perfit, and K. Rubin (2007), New insights into mid-ocean ridge volcanic processes from the 2005–2006 eruption of the East Pacific Rise, 9°46′N–9°56′N, *Geology*, *35*(12), 1079–1082, doi:10.1130/G23924A.1.

Sparks, R. S. J., H. Sigurdsson, and L. Wilson (1977), Magma mixing: A mechanism for triggering acid explosive eruptions, *Nature*, *267*, 315–318, doi:10.1038/267315a0.

Spence, W. (1987), Slab pull and the seismotectonics of subducting lithosphere, *Rev. Geophys.*, *25*(1), 55–69, doi:10.1029/RG025i001p00055.

Stakes, D., M. R. Perfit, M. A. Tivey, D. W. Caress, T. Ramirez, and N. Maher (2006), The Cleft revealed: Geologic, magnetic, and morphologic evidence for construction of upper oceanic crust along the southern Juan de Fuca Ridge, *Geochem. Geophys. Geosyst.*, *7*, Q04003, doi:10.1029/2005GC001038.

Stroup, D. F., D. R. Bohnenstiehl, M. Tolstoy, F. Waldhauser, and R. T. Weekly (2007), Pulse of the seafloor: Tidal triggering of microearthquakes at 9°50′N East Pacific Rise, *Geophys. Res. Lett.*, *34*, L15301, doi:10.1029/2007GL030088.

Sun, S. S., and W. F. McDonough (1989), Chemical and isotopic systematics of oceanic basalts: Implications for mantle composition and processes, in *Magmatism in the Ocean Basins*, edited by A. D. Saunders and M. J. Norry, *Geol. Soc. Spec. Publ.*, *42*, 313–345.

Tanaka, T., et al. (2000), JNdi-1: A neodymium isotopic reference in consistency with La Jolla neodymium, *Chem. Geol.*, *168*(3–4), 279–281, doi:10.1016/S0009-2541(00)00198-4.

Tegner, C., P. Thy, M. B. Holness, J. K. Jakobsen, and C. E. Lesher (2009), Differentiation and compaction in the Skaergaard Intrusion, *J. Petrol.*, *50*(5), 813–840, doi:10.1093/petrology/egp1020.

Todt, W., R. A. Cliff, A. Hanser, and A. W. Hofmann (1996), Evaluation of a ^{202}Pb–^{205}Pb double spike for high-precision lead isotope analysis, in *Earth Processes: Reading the Isotopic Code*, *Geophys. Monogr. Ser.*, vol. 95, edited by A. Basu and S. Hart, pp. 429–437, AGU, Washington, D. C.

Tolstoy, M., et al. (2006), A seafloor spreading event captured by seismometers, *Science*, *314*(5807), 1920–1922, doi:10.1126/science.1133950.

Toomey, D. R., G. M. Purdy, S. C. Solomon, and W. S. D. Wilcock (1990), The three-dimensional seismic velocity structure of the East Pacific Rise near latitude 9°30′N, *Nature*, *347*(6294), 639–645, doi:10.1038/347639a0.

Tormey, D. R., T. L. Grove, and W. B. Bryan (1987), Experimental petrology of normal MORB near the Kane Fracture-Zone: 22°–25°N, Mid-Atlantic Ridge, *Contrib. Mineral. Petrol.*, *96*(2), 121–139, doi:10.1007/BF00375227.

Vera, E. E., and J. B. Diebold (1994), Seismic imaging of oceanic layer 2A between 9°30′N and 10°N on the East Pacific Rise from two-ship wide-aperture profiles, *J. Geophys. Res.*, *99*(B2), 3031–3041, doi:10.1029/93JB02107.

Vera, E. E., J. C. Mutter, P. Buhl, J. A. Orcutt, A. J. Harding, M. E. Kappus, R. S. Detrick, and T. M. Brocher (1990), The structure of 0- to 0.2-m.y.-old oceanic crust at 9°N on the East Pacific Rise from expanded spread profiles, *J. Geophys. Res.*, *95*(B10), 15,529–15,556.

Villiger, S., O. Müntener, and P. Ulmer (2007), Crystallization pressures of mid-ocean ridge basalts derived from major element variations of glasses from equilibrium and fractional crystallization experiments, *J. Geophys. Res.*, *112*, B01202, doi:10.1029/2006JB004342.

Vlastélic, I., T. Staudacher, and M. Semet (2005), Rapid change of lava composition from 1998 to 2002 at Piton de la Fournaise (Réunion) inferred from Pb isotopes and trace elements: Evidence for variable crustal contamination, *J. Petrol.*, *46*(1), 79–107, doi:110.1093/petrology/egh1062.

Von Damm, K. L. (2004), Evolution of the hydrothermal system at East Pacific Rise 9°50′N: Geochemical evidence for changes in the upper oceanic crust, in *Mid-Ocean Ridges: Hydrothermal Interactions Between the Lithosphere and Ocean*, *Geophys. Monogr. Ser.*, vol. 148, edited by C. R. German, J. Lin, and L. M. Parson, pp. 285–304, AGU, Washington, D. C.

Von Damm, K. L., S. E. Oosting, R. Kozlowski, L. G. Buttermore, D. C. Colodner, H. N. Edmonds, J. M. Edmond, and J. M. Grebmeier (1995), Evolution of East Pacific Rise hydrothermal vent fluids following a volcanic eruption, *Nature*, *375*(6526), 47–50, doi:10.1038/375047a0.

Walczyk, T. (2004), TIMS versus multicollector-ICP-MS: Coexistence or struggle for survival?, *Anal. Bioanal. Chem.*, *378*, 229–231, doi:10.1007/s00216-003-2053-4.

Walder, A. J., I. Platzner, and P. A. Freedman (1993), Isotope ratio measurement of lead, neodymium and neodymium samarium mixtures, hafnium and hafnium lutetium mixtures with a double focusing multiple collector inductively coupled plasma mass-spectrometer, *J. Anal. At. Spectrom.*, *8*(1), 19–23, doi:10.1039/ja9930800019.

White, S. M., R. M. Haymon, D. J. Fornari, M. R. Perfit, and K. C. Macdonald (2002), Correlation between volcanic and tectonic segmentation of fast-spreading ridges: Evidence from volcanic structures and lava flow morphology on the East Pacific Rise at 9°–10°N, *J. Geophys. Res.*, *107*(B8), 2173, doi:10.1029/2001JB000571.

White, S. M., R. M. Haymon, and S. Carbotte (2006), A new view of ridge segmentation and near-axis volcanism at the East Pacific Rise, 8°–12° N, from EM300 multibeam bathymetry, *Geochem. Geophys. Geosyst.*, *7*, Q12O05, doi:10.1029/2006GC001407.

Wilcock, W. S. D., S. D. Archer, and G. M. Purdy (2002), Microearthquakes on the Endeavour segment of the Juan de Fuca Ridge, *J. Geophys. Res.*, *107*(B12), 2336, doi:10.1029/2001JB000505.

Wilcock, W. S. D., E. E. E. Hooft, D. R. Toomey, P. R. McGill, A. H. Barclay, D. S. Stakes, and T. M. Ramirez (2009), The role of magma injection in localizing black-smoker activity, *Nat. Geosci.*, *2*, 509–513, doi:10.1038/NGEO1550.

Wright, T. L. (1973), Magma mixing as illustrated by the 1959 eruption, Kilauea Volcano, Hawaii, Geol. *Soc. Am. Bull.*, *84*(3), 849–858, doi:10.1130/0016-7606(1973).

Wright, T. L., and R. T. Okamura (1977), *Cooling and Crystallization of Tholeiitic Basalt, 1965 Makopuhi Lava Lake, Hawaii*, *Geol. Surv. Prof. Pap.*, *1004*, 78 pp.